Increasing Turbine Hall Safety by Using Fire-Resistant, Hydrogen-Containing Lubricant Cooling Liquid for Rotor Steel Mechanical Treatment

Alexander I. Balitskii [1,2,*] , **Maria R. Havrilyuk** [1] , **Valentina O. Balitska** [3] , **Valerii O. Kolesnikov** [1,4] **and Ljubomyr M. Ivaskevych** [1]

1   Department of Strength of the Materials and Structures in Hydrogen-Containing Environments, Karpenko Physico-Mechanical Institute, National Academy of Sciences of Ukraine, 5 Naukova Str., 79-601 Lviv, Ukraine

2   Department of Mechanical Engineering and Mechatronics, West Pomeranian University of Technology in Szczecin, 19 Piastow av., 70-310 Szczecin, Poland

3   Department of Physics and Chemistry of Combustion, Lviv State University of Life Safety, 35 Kleparivska, 79-000 Lviv, Ukraine

4   Department of Production Technology and Professional Education, Taras Shevchenko National University of Lugansk, Kovalya Str. 3, 36-000 Poltava, Ukraine

*   Correspondence: balitski@ipm.lviv.ua

Abstract: This paper is devoted to the development of hydrogen-containing, environmentally safe, fire-resistant, and corrosion-protected lubricant cooling liquids (LCLs) from vegetable oils with improved sanitary and hygienic parameters for the machining of parts and equipment made from high-strength steels for application during the interoperation period in turbine halls. The use of plant raw materials as ecologically and fire-safe LCLs increased the efficiency of LCLs when evaluating drilling steel in terms of the dependence of the stability of the cutting tool on the drilling speed. Chips formed from LCLs during turning had a compact, cylindrical appearance, and the addition of both water and coolant during turning significantly changed the morphology of the cutting particles. Using water and LCL intensified the physical and chemical destruction processes. After the use of water and LCL, the concentration of hydrogen in the cutting products of 38KHN3MFA steel increased, which indicated its participation in facilitating the destruction during machining. In the chips formed when using LCL, the amount of hydrogen increased by 2.25 times compared to the chips obtained with the dry treatment, while with coolants, it increased by 2.6 times, indicating the intense flow of decomposition products of LCL through diffusion processes in the cutting zone. Hydrogen reduces the energy costs for the destruction of structural and phase components and promotes their dispersion. The creation of 2D and 3D images allowed for a more detailed approach to the study of the influence of LCL on surface treatments.

Keywords: high-strength steels; environment-friendly, green lubricating and cooling liquids; mechanical treatment; rapeseed; sunflower oils

1. Introduction

The modern, high-alloyed, high-strength steels applied in the energy sector combine high strength, plasticity, a tendency toward hardening, and low thermal conductivity. They are very hard to machine. For quality machining of complex alloyed steels, the use of LCL water emulsion holds great potential. Its advantages include relatively lower cost, lower toxicity, and much better cooling capacity compared to oil, as well as fire safety [1–54]. One approach to this complex, technical situation involves using sunflower and rapeseed vegetable oils for LCL synthesis. To reduce environmental pollution and workers' exposure in industry, it is possible to replace petroleum oils with vegetable oils in the LCL used in technological processes in turbine halls. Ensuring reliable and high-quality

corrosion protection of machined parts and equipment during and between operations and simultaneously reducing the temperature and energy mechanical parameters when machining high-strength, complex, alloyed steels for power generation is an important topical problem that can be addressed through the development of environmentally safe, aqueous LCL. The originality of the present study lies in the fact that the microreliefs of surfaces in connection with the initial microstructure and the obtained cutting products have not been analyzed for lubricating cooling liquids. The formation of cutting products is significantly influenced by both technological factors, such as the speed of rotation, and the physical and chemical characteristics of lubricating coolants. They help increase the corrosion resistance of products, as well as the shavings themselves, which can be sent for recycling. If the shavings contain rust, the amount of soot in the shavings during metallurgical production increases. If the processing is carried out with lubricating fluids produced on the basis of petroleum oil, there will be more environmental problems during the processing of chips in comparison to processing chips obtained using ecologically clean oil.

2. Literature Survey: State of the Art

Recently, the interest of scientists and consumers in the practical use of vegetable oils as bases and additives for lubricants and mineral oils has increased. To investigate this possibility, various methods have been used, such as the selection of additives, chemical modification of vegetable oils, and even genetic modification of plant seeds [1–6].

The investigation of the use of plant raw materials as ecologically and fire-safe LCLs is an important component of modern scientific research in the USA, South Korea, Malaysia, India, Ukraine, Turkey, Poland, and other countries [7–95].

Vegetable oils are mainly triglycerides: triple esters of long-chain carboxylic (fatty) acids with glycerol. Most of these oils contain at least 4, and sometimes up to 12, different fatty acids. The authors of several publications [1–25] have shown that vegetable oils can effectively replace petroleum oils in lubricants and confirmed this perspective. In these studies, attention was paid to castor, rapeseed, soya, palm, and coconut oils.

The use of LCL during metal machining increases the stability of the cutting tool, improves the quality of the machined surface, and reduces the cutting force. There are requirements for the quality of LCLs: exertion of a protective effect during inter-operational storage of parts; no foaming during operation; stability during storage and transportation and at low temperatures; satisfactory cleaning properties; long service life for water LCLs; ease of preparation of emulsions in water with different hardness levels; satisfactory decomposition of the spent solid waste during disposal; environmental safety for the waste; and fire safety [15,24,96–120].

Oil modification is widely used to improve the operational properties of LCLs. The most common methods are saponification, methanolysis, and sulfidation of technical oils [17,19,120–123]. Soap is obtained from castor, rape, and mustard oils. Long and polar fatty acid chains form oriented molecular films that interact with metal surfaces, reducing their friction and wear.

During transesterification due to the replacement of acid groups in the ester molecule or of alcohol groups, this ester is converted into another ester. To obtain a high yield of the necessary ester, alcohol is added in excess. The advantage of this technique is that it makes it possible to obtain esters directly from oil without carrying out an intermediate operation.

The most rational methods are the use of vegetable oils as dispersion media and their soaps as thickeners and the implementation of chemical modifications to obtain effective anti-wear and protective additives [1–23].

Rotor manufacturing technology involves the turning and drilling of the workpiece, for which it is necessary to use LCLs [20–23,118–123]. The use of LCLs is also necessary during planned and emergency repairs after operational damage.

Steam turbine rotors have rotation speeds of 3000 min^{-1} (RPM) and more. Centrifugal forces due to the rotation of a massive rotor cause stress in its parts. Solid turbine rotors,

blades, shafts, and disks are the most loaded elements of turbines. As the turbine unit power increases, the loads on all its parts and components increase and, thus, the requirements for the steels and alloys from which they are made increase.

The high degree of alloying of steels and alloys has a significant impact on their machinability due to the formation of dispersed phases based on alloying elements, strengthening solid solutions, and structure components: carbides, nitrides, and intermetallic compounds. Furthermore, the development of modern information technologies has had a significant impact on the paradigm employed in modern research on the mechanical processing of materials [107–145].

3. Formulation of the Problem: Materials and Methodology

For research, three LCL samples were chosen: ET-2 petroleum oil (LCL_o) and newly synthesized LCLs based on sunflower (LCL_s) and rapeseed (LCL_r) oils.

Transesterification is carried out using methyl or ethyl alcohols that can form complex esters. We used amino alcohol (TEA) as an alcohol and adjusted the reaction conditions accordingly. The transesterification reaction of TEA with sunflower (rapeseed) oil was carried out in the presence of a solution of potassium hydroxide (KOH). The reaction proceeded gradually as follows: (1) oil triglycerides were saponified with KOH; (2) TEA hydrolyzed and saponified the oil triglycerides; and (3) alcoholysis of TEA oil triglycerides occurred in the presence of a catalyst—methyl alcohol in component mass ratios from 4:1 to 5:1 at temperatures from 95 to 125 °C. Samples of LCL concentrates were obtained by modifying vegetable oils as follows. Calculated amounts of oil, TEA, 35–45% potassium hydroxide, and methyl alcohol were sequentially loaded into a flask equipped with a stirring and heating device. With continuous stirring, the reaction mixture was heated to 95–125 °C over 2–4 h and appropriate amounts of neonol A9-4 and sunflower oil were added. Everything was stirred for 1–2 h and analyzed.

The LCLs for testing were prepared in two stages: preparation of the water and mixing of the concentrate with water. For the LCL tests, a 3% emulsion was prepared by mixing the concentrate in appropriate proportions with mineralized water with a hardness of 7 mg-eq/l, which was prepared by dissolving 600 mg of magnesium sulfate (hemihydrate) and 124 mg of calcium chloride (anhydrous) in 1 L of distilled water. The physicochemical characteristics of the LCLs were determined (appearance, pH, aggregate stability, density).

The appearance of the samples was assessed visually—they appeared as homogeneous liquids, beige in color. All the LCL samples presented specific, non-irritating smells of the corresponding oils, as determined organoleptically.

The effectiveness of the LCLs based on synthesized concentrates was evaluated in terms of the influence of a working fluid with a mass fraction of 3% of the concentrate on the performance of mechanical processing (drilling speed) and on tool wear (total depth of the drilled holes before the tool became blunted).

For the determination of the marginal wetting angles of the liquids, quantitative evaluation of the effects of the LCLs on wetting was carried out by changing the marginal wetting angles [22–24]. The sample, which was made of 38KHN3MFA steel in the form of a plate (1.5×2.0 cm^2) with a surface roughness of 0.63 μm, was placed on a stage, the height of which was adjusted with the help of a screw to bring it to the level of the focus of the camera.

Mineralized water (hardness: 7.0 mg-eq/L), LCL_o, and the synthesized LCLs were compared. A drop of the studied liquid (with a diameter of no more than 3 mm) was applied with a syringe to the prepared surface of the sample, holding the syringe at an angle of 15 to 25° from the surface. The drop was photographed and the image was processed using the Dopel Illustrator program, and then the angle was measured and its cos determined.

The postoperative protective effect was evaluated from the appearance (presence of traces of corrosion) of the 38KHN3MFA steel chips after turning in water and the LCL following 100 h of storage in a desiccator with water.

The efficiency of the LCLs when drilling steel was evaluated by establishing the dependence of the stability of the cutting tool on the drilling speed. When drilling, we used drills made of high-speed P6M5K5 steel alloyed with 5% cobalt (HSS COBALT DIN 338 manufactured by IRVIN, Germany). The cutting surface of the drills was ground at an angle of 135°.

Samples of 38HN3MFA steel in the delivery state (the initial state condition) with a hardness of 35 HRC were investigated (Tables 1 and 2) [23].

Table 1. Chemical composition of steels (wt., %, Fe—balance).

Steel	C	Si	Mn	Cr	Ni	P	S	V	Mo	Cu
38KhN3MFA	0.39	0.26	0.48	1.30	3.20	0.008	0.003	0.15	0.42	0.23

Table 2. Mechanical and physical properties of steels.

Steel	Yield Strength, σ_T, MPa	Ultimate Tensile Strength, σ_T, MPa	Elongation, δ, %	Reduction in Area, ψ, %	Fracture Toughness K_{Ic}, MPa$\sqrt{m}$
38KhN3MFA	807	955	17	51	184

The chips were obtained by cutting cylinders with a diameter of 28 mm and a thickness of 4 mm from the workpiece. The cutter was equipped with a VK-6 carbide insert. To create equal turning conditions, the cutter was sharpened and the same angle between it and the workpiece was used. Experiments were carried out dry during grinding with water and coolant containing sunflower oil at 200 and 315 RPM.

The microstructure parameters of the steel were determined with a LOMO ES METAM RV 21 microscope. To obtain micro-grinds, etching was used with 4% nitric acid solution. The features of the chip morphology were studied with a ZEISS Stemi 2000C microscope. This microscope was equipped with a SIGETA International Color Digital Camera MCMOS 5100 5.1 MP.1. An EVO-40XVP electron microscope with an INCA Energy 350 Microanalysis System was also used. The Gwyddion software packages were used to build images of the 2D and 3D surfaces. The computer software packages Gwyddion 2.61 and 2.62 are freely downloadable as open-source code [28]. The most popular versions of these computer packages are versions 2.2 and 2.5, and the developers are Petr Klapetek and David Nečas. The installation file is called gwyddion.exe. The latest version of this computer program can support both 32 bit and 64 bit Windows XP/Vista/7/8/10/11 operating systems. Gwyddion is a modular computer program that can be used for scanning probe microscopy (SPM) data analysis and visualization. The computer program is intended for analysis of height fields, which are obtained with scanning probe microscopy methods (STM, SNOM/NSOM, MFM, AFM). However, in principle, this program can be used to analyze any kind of elevation field or image; for example, profilometry data. The hydrogen concentration in the chips was determined using an ONH-836 Leco analyzer as described in [21].

4. Results and Discussions

LCL tests were performed on 38KHN3MFA rotor steel samples with the typical microstructure (Figure 1). For the microstructure investigation (determination of the area and the length of the structural components) the adequate program was used [29].
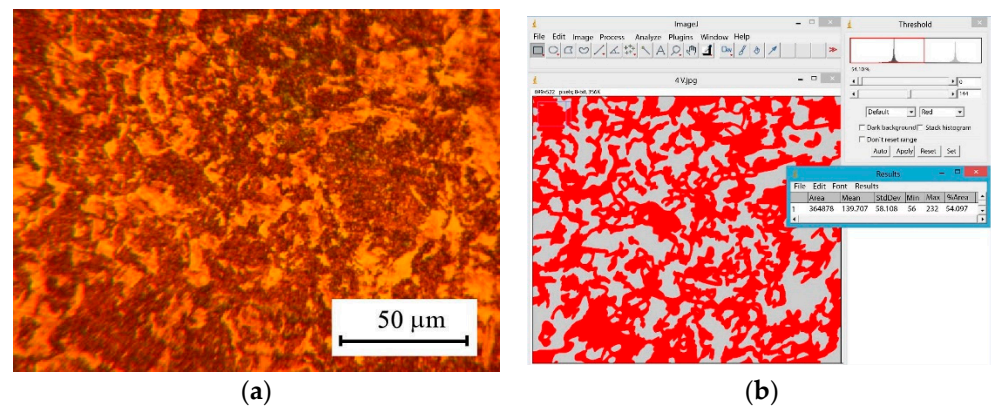
Figure 1. The microstructure of the 38KhN3MFA steel sample (initial state condition) (**a**) and the appearance of the ImageJ program dial window (**b**) (the area of the pearlite structural component is shown in red).

Analysis of the histograms (Figure 2) showed that the area distribution of ferrite colonies was in a range (Figure 2a) from 0 to 1000 pixels^2, and the maximum value of the distribution curve was 125 pixels^2. For pearlite colonies, the largest area was occupied by colonies with areas of up to 2000 pixels^2 (Figure 2b). The maximum value of the distribution curve was 1600 pixels^2. The length distribution of ferrite colonies was between 1 and 20 μm (Figure 2c), with the maximum value of the distribution curve at 7.5 μm. For the pearlite component, from 10 to 40 μm (Figure 2d), the maximum value of the distribution curve was 18 μm.
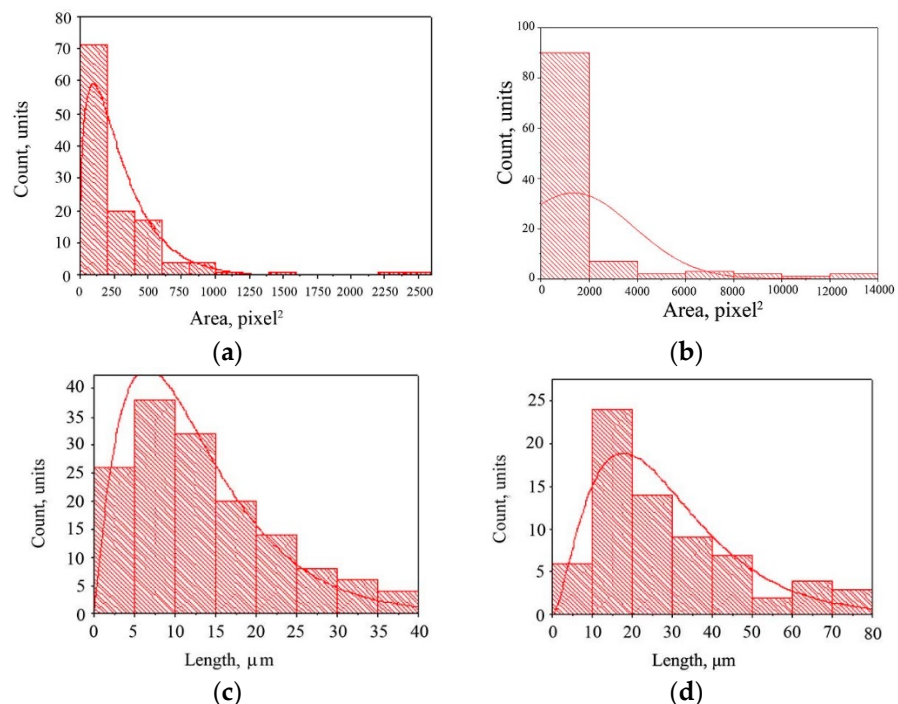

Figure 2. Histograms with normal distribution curves highlighting the calculated data: the area occupied by ferrite (**a**) and pearlite (**b**) colonies (pixels^2) and the linear dimensions of ferrite (**c**) and pearlite (**d**) colonies. Schemes follow the same formatting.

When studying the effects of LCL on the mechanical processing of 38KhN3MFA steel, it was necessary to take into account the angle of wetting of the steel surface by the drops of LCL. This LCL measurement makes it possible to assess the wettability of the surface with a liquid and, accordingly, its ability to penetrate into the zone of mechanical processing.

The penetration of LCL depends on its nature and can lead to passivation or increased corrosion of steel. In this case, mechanical processing was greatly facilitated due to the cooling of the surfaces and the formation of a film that separated the processed surfaces. The marginal wetting angles of LCL_s, LCL_r, and LCL_o at T = 293 K with 38KHN3MFA steel were determined according to the methodology. For one of the LCLs (Figure 3), the wetting angle was almost three times smaller than the wetting angle of water, and that of LCL_r was 1.75 times smaller, allowing significant permeability into the treatment zone.
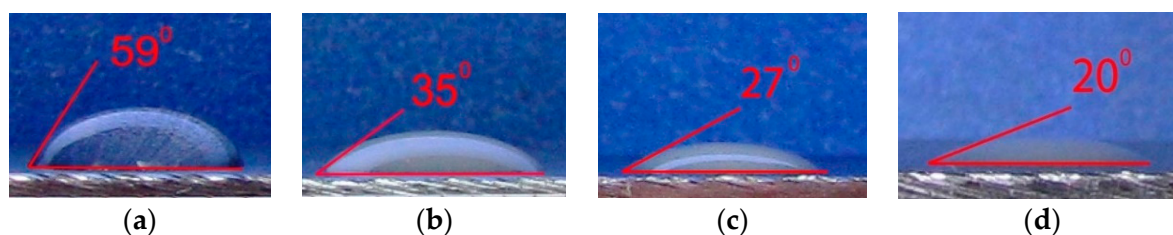

Figure 3. Wetting angles of water (**a**), LCL_o (**b**), LCL_r (**c**), and LCL_s (**d**).

The postoperative protective effect of LCL_s, assessed by the appearance of the chips—the "indicator"—after 100 h (absence of traces of corrosion on the chip, Figure 4) following turning confirmed the reliability of its protective action [30,141,145].
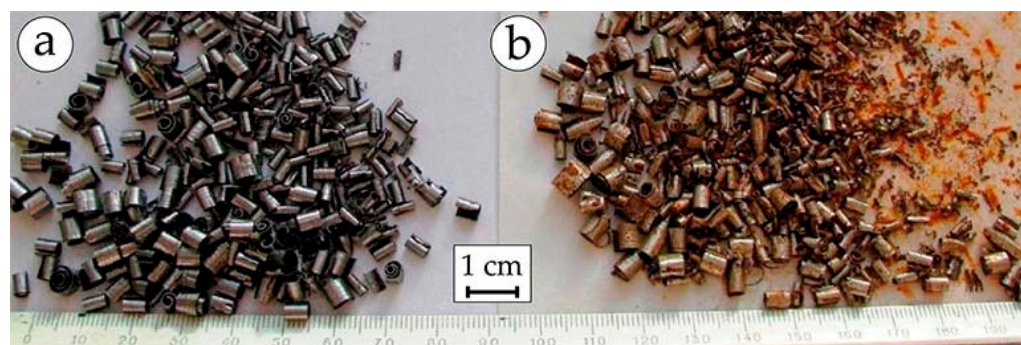

Figure 4. View of steel chips following turning in LCL_s (**a**) and water (**b**) after 100 h.

The small angle of wettability of the LCLs with the steel surface ensured better penetration into the processing zone and verified the protective effect of 38KHN3MFA steel.

When turning a sample of 38KHN3MFA steel, the amount of tool wear decreased by a factor of almost 2 when LCL_s and LCL_r were used for 10 min compared to LCL_o (Figure 5a), and when changing the chemical composition of LCL_o to that of LCL_s or LCL_r at a concentration of 3%, the duration of the drilling of the steel samples increased by 60% (Figure 5b).

The estimation of the resource change in the tool during drilling and the precision of the 38HN3MFA steel samples indicated that, depending on the liquid used (Figure 5b), increases in LCL_s and LCL_r concentrations by 2.5 times led to an increase of only 11%. Therefore, LCL_s increased the durability of the tool when turning and drilling 38KHN3MFA steel by ~1.6 times and 60%, respectively.

The fire-resistant 3% aqueous LCL_s and LCL_r obtained on the basis of the TEA transesterification reactions of triglycerides of sunflower and rapeseed oils facilitated turning and drilling processes with 38HN3MFA steel and provided protection for the parts against corrosion in the interoperation period after processing.
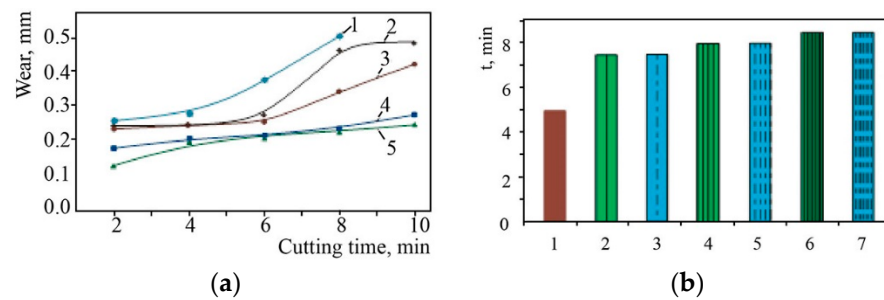
(a)　　　　　　　　　　　　(b)

Figure 5. Dependence of the tool wear on the duration of the turning of 38KhN3MFA steel: (1) dry, (2) water, (3) LCL_o—3%, (4) LCL_r—3%, (5) LCL_s—3%. Turning mode: workpiece diameter—25 mm; speed—200 rpm, feed—0.53 mm (**a**). Dependence of the duration of the drilling of 38KHN3MFA steel on the composition of LCL: (1) LCL_o—3%; (2, 4, 6) LCL_s—2%, 3%, and 5%; (3, 5, 7) LCL_r—2%, 3%, and 5%. Drilling modes: drill with a diameter of 12.7 mm; number of revolutions—180 rpm (**b**).

In Table 3, the values for the roughness and hydrogen content in the chips are given. Figure 6 shows the cutting surfaces with dry cutting conditions and with water when using LCL containing rapeseed and petroleum sunflower oil.

Table 3. Effects of cooling media on surface roughness of steel samples and hydrogen content in chips after turning.

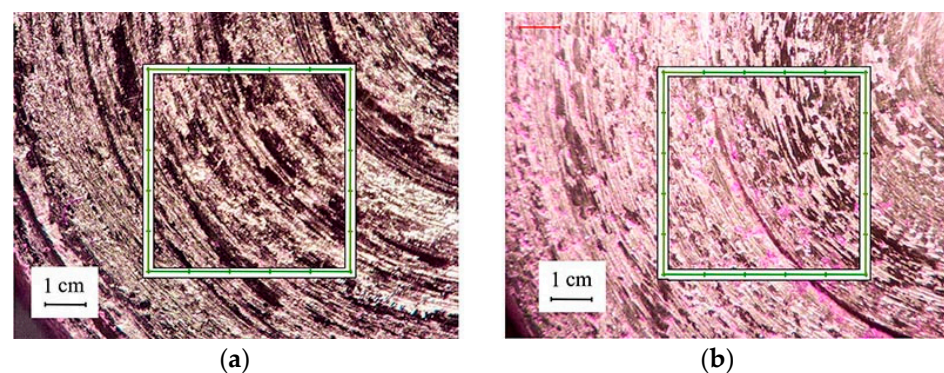| N	Experiments	Rz	C_H (ppm)
1	Air	37.08	0.88
2	Water	5.01	3.14
3	LCL_s	4.43	7.22
4	LCL_r	5.52	7.47
5	LCL_o	6.36	7.83

(a)　　　　　　　　　　　　(b)

Figure 6. Cutting surfaces of 38KhH3MFA steel samples: dry (**a**); with water (**b**). The squares indicate the areas for the reproduction of 2D and 3D images measuring 5 by 5 cm, depending on the value.

As can be seen from Table 3, the highest roughness was observed for dry cutting. The use of water significantly reduced the roughness. However, the use of water for this steel also led to the appearance of corrosion damage (Figure 6b). To prevent the occurrence of corrosion processes and their development, it is advisable to use LCLs.

Figure 6 shows the surfaces of the samples after dry turning and turning with water, where the squares mark the areas with which 2D and 3D surface visualization was undertaken.

The surface with the highest roughness Rz = 37 μm was formed during dry cutting (Table 3, Figures 6a and 7a,b). Figure 4b shows the corrosion damage on the surface after

turning with water. Cutting with water and LCL improved the machined surface and significantly reduced roughness (Rz = 4–7 μm).
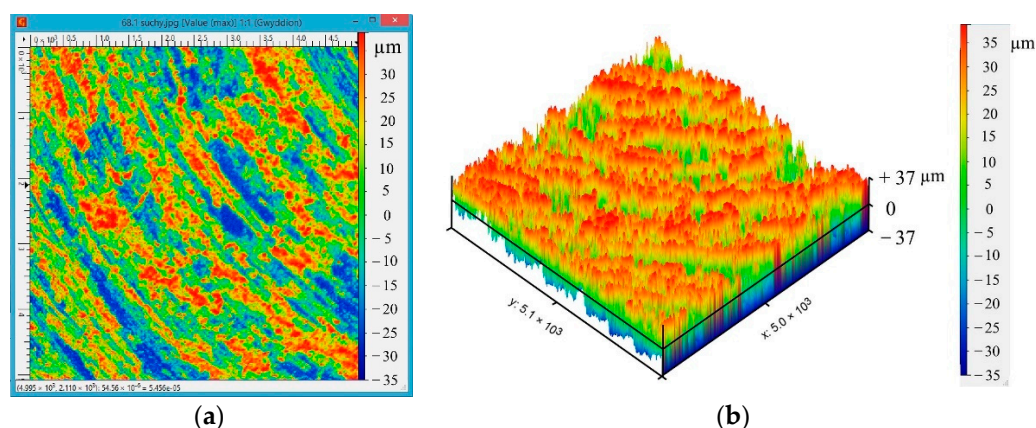

Figure 7. Dry cutting surfaces of 38KHN3MFA steel samples: 2D visualization (**a**) and 3D visualization (**b**) in the Gwyddion computer package.

Comparing Figure 7a,b and Figure 8a,b makes it possible to see that, during dry cutting (Figure 5a), there were "deep tears" (blue color). In Figure 6b, it can be seen that the surface layer was more uniform and did not have deep eddies. The average surface roughness during dry processing was 37 μm (Table 1). For the surface treatment with water, most of the surface is shown in orange colors and the roughness was in the range from 2 μm to 6 μm, with an average roughness of 5 μm (Figure 8a); that is, most of the treated surface, in contrast to the dry treatment, did not show the same differences and aggravation. The Gwyddion 2.61 computer package has downloaded from the following website: http://gwyddion.net/download.php (accessed on 27 November 2022). We did not develop any additional algorithms when using this package. The developers of this free software are David Nečas and Petr Klapetek. The installation file is named gwyddion.exe. The latest version of the program is supported by Windows XP/Vista/7/8/10/11 and can be used for both 32 and 64 bit computer systems.
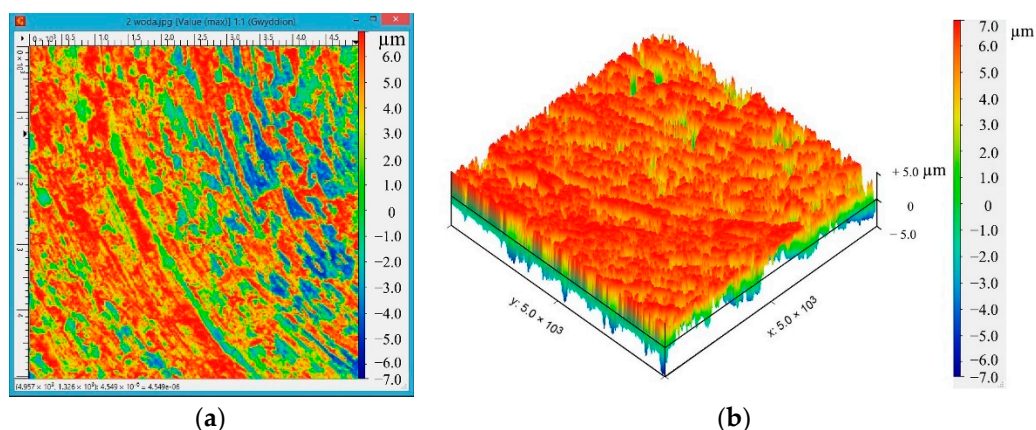
Figure 8. Cutting surfaces of 38KHN3MFA steel samples with water: 2D visualization (**a**) and 3D visualization (**b**) in the Gwyddion computer package.

Gwyddion is a modular computer program for visualization and analysis of scanning probe microscopy (SPM) data. It is intended mainly for analysis of height fields obtained with scanning probe microscopy methods (AFM, SNOM/NSOM, STM, MFM). Its advantage is that it can also be used to analyze any other kind of height field or image; for example, profilometry data (http://gwyddion.net (accessed on 25 Decem-

ber 2022)). Tutorials on how to use different versions of Gwyddion can be found at at: http://gwyddion.net/presentations/tutorials.php (accessed on 25 December 2022). [26].

As shows the XVP scanning electron microscope data and indicates a positive effect from LCLs and LCLr on the machining quality of 38KhN3MFA steel samples after sharpening with the LCLs (Figure 9).
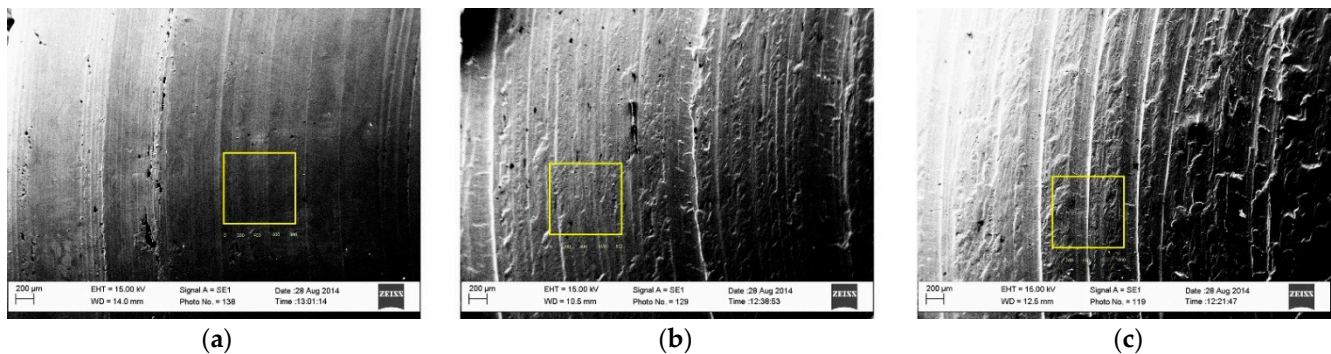

(a)   (b)   (c)

Figure 9. Surfaces of 38KhN3MFA steel samples after turning during LCL cutting (selected areas for visualization—800 from 800 μm): LCL_s (**a**); LCL_r (**b**); LCL_o (**c**).

Areas from which the reconstructions of 2D and 3D surfaces were produced, taking into account the value of the surface roughness, are marked in yellow. From Figures 10–12, it can be seen that cutting with LCL_s and LCL_r resulted in a smoother and more "even" surface. The roughness was in the range of 4.4 to 6.5 microns. The color ranges for LCL_s and LCL_r were more uniform (Figures 10a and 11a) than for LCL_o, where, in addition to green and blue colors, there were red and yellow colors (Figure 12a). To reproduce the microrelief of the surface treated with LCL_s, a smooth surface with a small difference in roughness corresponding to −1 μm to +2 μm (shown in green color with the largest peaks corresponding to +2 μm) was obtained, and the blue surface corresponds to −3.0 to −6.0 μm (Figure 10a,b). The color ranges for LCLs and LCL_r were more uniform (Figures 10a and 11a) than for LCL_o, where, in addition to green and blue colors, there were red and yellow colors (Figure 12a). The largest peaks during processing with LCL_r reached sizes of up to +7 μm and were distributed over the entire surface very evenly (Figure 11a,b). The microrelief of the reverse surface in the left part of the image was in the range from −2 μm to +2 μm and had a more or less uniform distribution, indicated by the green color scale. The right part of the image is shown in blue-green colors, which correspond to −2 μm to −5 μm. The petroleum oil in the composition of LCL_o contributed to the appearance of a sharper microrelief (Figure 12), where there were areas with protrusions that had a sharp shape (Figure 12b). The central ridge had external elevations from +3 to +7 microns (Figure 12) and a large number of single peaks between −2 and +6 microns. On both sides of the ridge, there were depressions ranging from −2 to −7 microns scattered over the entire area. For the selected areas after treatment with sunflower and rapeseed oils, the numbers of dense peaks (Figures 10b and 11b) were significantly smaller.

The largest amount of hydrogen, which was obtained after the analysis of the chips, was recorded for LCL_o (C_H = 7.83 ppm). An increase in the amount of hydrogen can also contribute to the processes of destruction of the surface and subsurface layers under cutting conditions.

Transitions to alloys in which the area of pearlite prevails over the ferrite component lead to the production of shorter chips, which is due to the strengthening of the metal matrix and the increase in the number of grains and alloyed carbide phases. The number of fracture chips also increases; i.e., macrocracks do not develop as intensively as for alloys where ferrite occupies a larger area than pearlite [27].
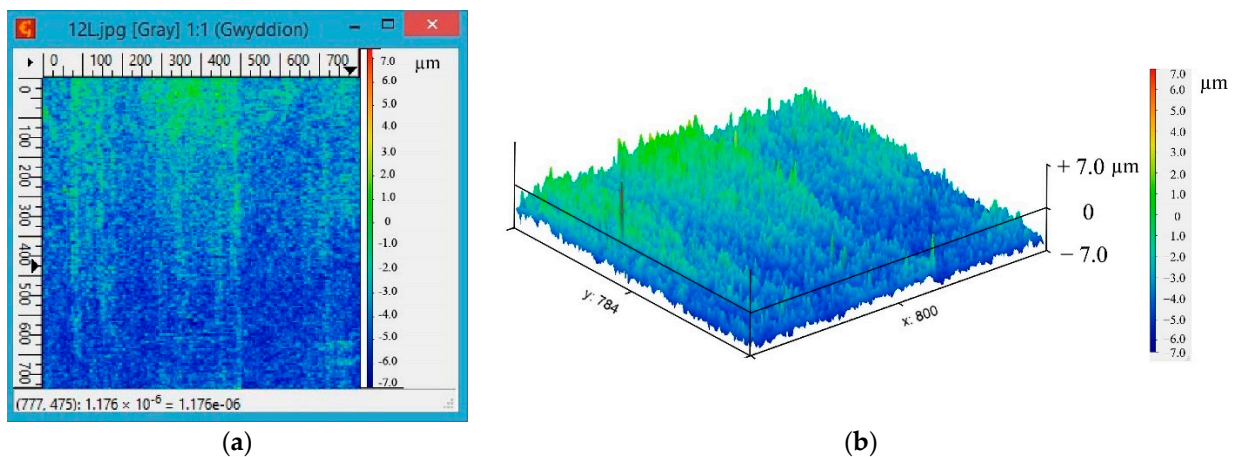
Figure 10. Surface area treated with LCL$_s$: 2D (**a**) and 3D (**b**) images of the surface.
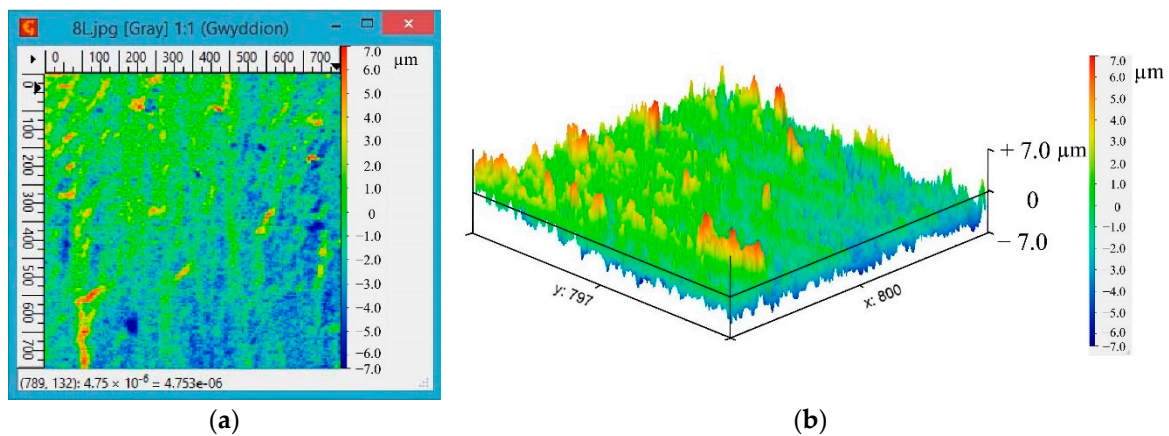
Figure 11. Surface area treated with LCL$_r$: 2D (**a**) and 3D (**b**) images of the surface.
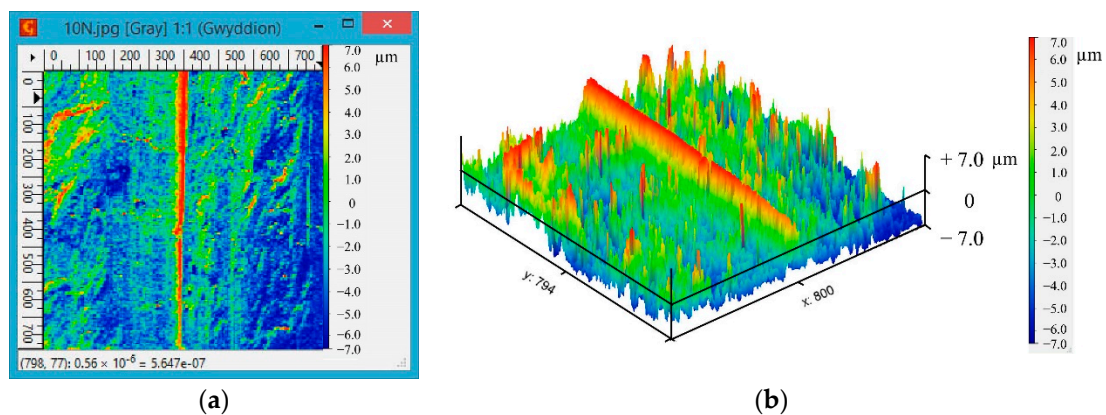
Figure 12. The area of the surface that was processed when applying LCL$_o$: 2D (**a**) and 3D (**b**) images of the surface.

Figures 13 and 14 shows graphs of changes in surface roughness depending on the change in the average size of the ferrite colonies. The experiments were carried out on 38KhN3MFA steel samples (see Tables 1 and 2). The following trend was observed: the finer the grain size, the lower the surface roughness.

Figure 13. Influence of ferrite colony size on the surface roughness of 38KhH3MFA steel under dry friction conditions.

Figure 14. Influence of ferrite colony size on the surface roughness of 38KhH3MFA steel under lubrication conditions.

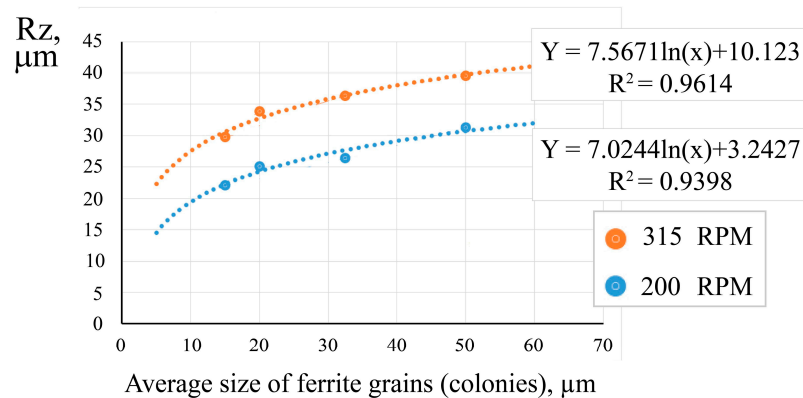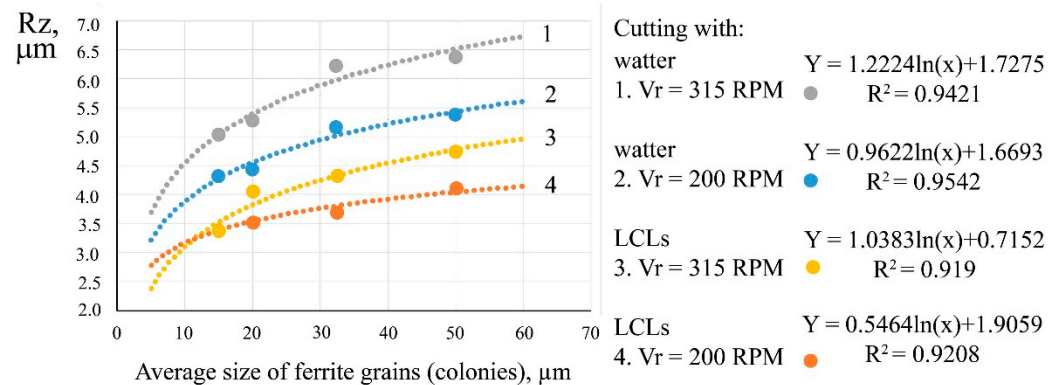Samples where the area of the pearlite component was dominant had finer chips than those samples where ferrite was the dominant component. According to established ideas, a macrocrack forms in front of the cutter and, because of the increased brittleness of the alloy, much finer chips are produced. When using water and LCL, physicochemical processes of destruction occur that affect the morphology of the chips. The chips become more compact and take on a rounded shape. Since ferrite belongs to the plastic phase and pearlite to the brittle phase, the correction of the structural-phase alloy affects the numbers of brittle- or viscous-type fractures.

Figures 15–17 show the image of chips formed during the turning of 38KhH3MFA steel in various environments. Some fragments of the chips obtained during dry turning contained varying colors (Figure 15a,b), which indicated the occurrence of oxidation processes due to an increase in temperature. When using water and LCL, the number of such chips was significantly reduced.

Chips formed during turning with water demonstrated local corrosion damage, as well as cracks and cuts, both on the inner and outer sides (Figure 16a,b). The appearance of corrosion damage on the surface of the chips was recorded immediately after the experiment. Cracks were observed on the chips, the banks of which showed corrosion damage.

Under the influence of a corrosive environment, the growth and propagation of cracks intensified. The chips formed during turning with LCLs had a compact cylindrical appearance (Figure 17a,b). The addition of both water and coolant during turning significantly changed the morphology of the cutting particles: they were crushed, and a large number of spiral-shaped particles with local deformation that were elongated along the axis appeared.
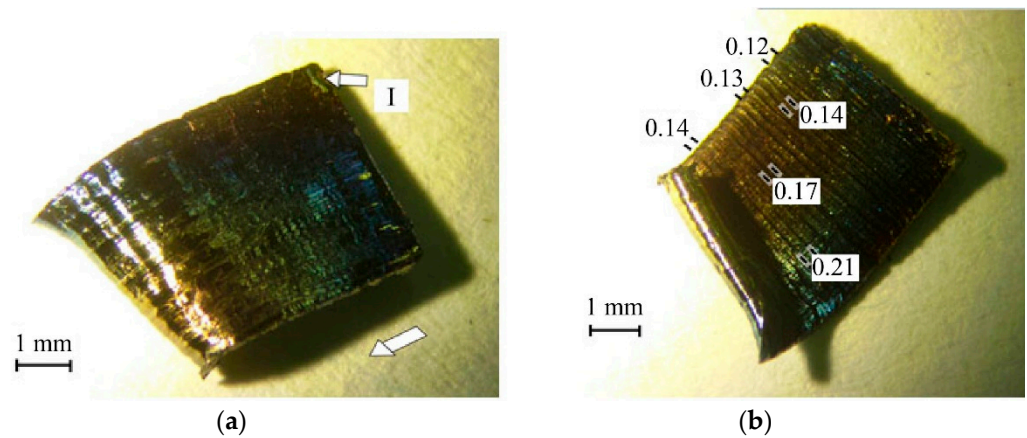
Figure 15. Chips generated during dry turning (demonstrating varying colors): outside (**a**); inside (**b**).
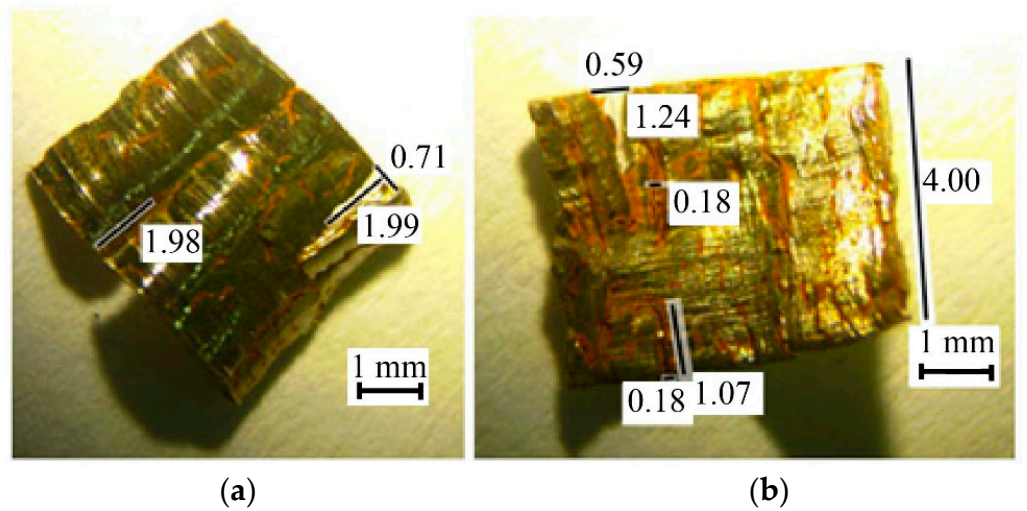

Figure 16. Chips formed during turning with water (demonstrating corrosion damage): outside (**a**); inside (**b**).
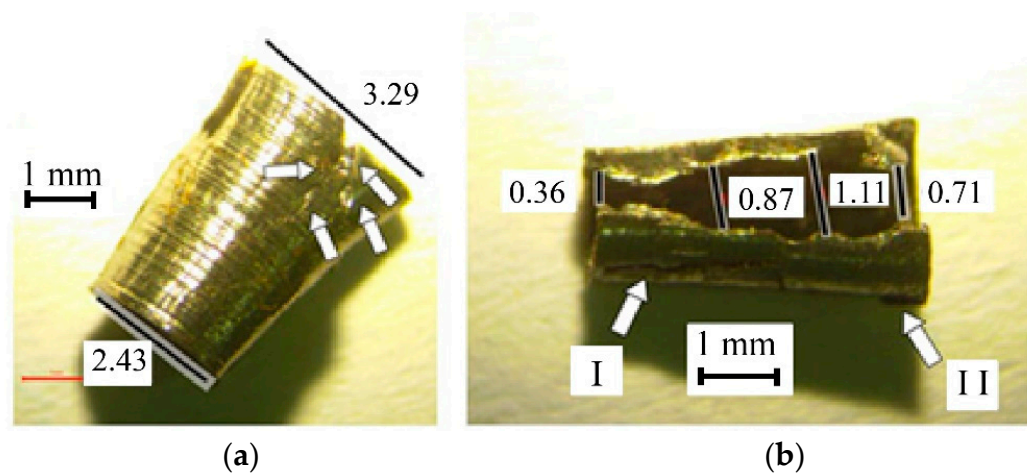

Figure 17. Chips formed during turning with LCLs: outside (**a**); inside (**b**).

The lower parts of the chips (Figure 17a) had a smaller diameter (2.43 mm) than the upper parts (3.29 mm). The arrows in Figure 17b show the damage on the surface of the

chips, which appeared in semi-cylindrical, not completely closed shapes and had widths of 0.36 to 1.1 mm.

Chip curling is an important safety factor for service personnel in machining.

5. Fire Security when Applying LCL in Turbine Halls according to EU Normative Requirements

Due to the incidence of ruptures in rotors and retaining rings caused by accidents, it is necessary to improve the safety of repair procedures in the turbine halls of energy units. For example, in one instance, a fragment of a hydrogen-cooled TG retaining ring pierced the fiberglass cylinder, as a result of which transformer oil began to flow under pressure into the gap between it and the rotor, which caused the formation of an air–hydrogen–oil mixture and the occurrence of a hydrogen fire with an explosion. One of these cracks, having reached a critical size, led to the instantaneous brittle failure of the generator shaft along the fan seat flange. This caused the processional movement of the TG rotor and the appearance of additional braking and transverse forces in the medium-pressure and low-pressure cylinders of the turbine, which resulted in shaft separation. Thus, the hydrogen-cooled TG was completely destroyed, and the rotor shaft was divided into four parts. Increasing turbine- and machining-hall safety by using fire-resistant hydrogen-containing lubricating and cooling liquid for mechanical treatment of high strength steels involves various technological processes, such as removing the rotor from a TG (Figure 18a,b); NDT testing of damaged TG rotors (Figure 18c) and the damaged outer (Figure 18d) and inner (Figure 18e) surfaces of retaining rings; application of fire-resistant LCL in the TA during repair (Figure 18e) with possible increased hardness (Figure 18g,h); and the assembly of hydrogen-cooling channels (Figure 18i) and retaining rings after repair (Figure 18j) [93]. The advantage of the use of LCL from vegetable oils is their rapid biodegradation in natural conditions; in contrast to petroleum oils, this makes it possible to reduce environmental pollution and increase fire and explosion safety.

(a)
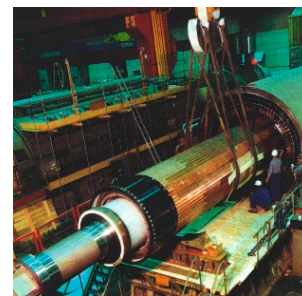
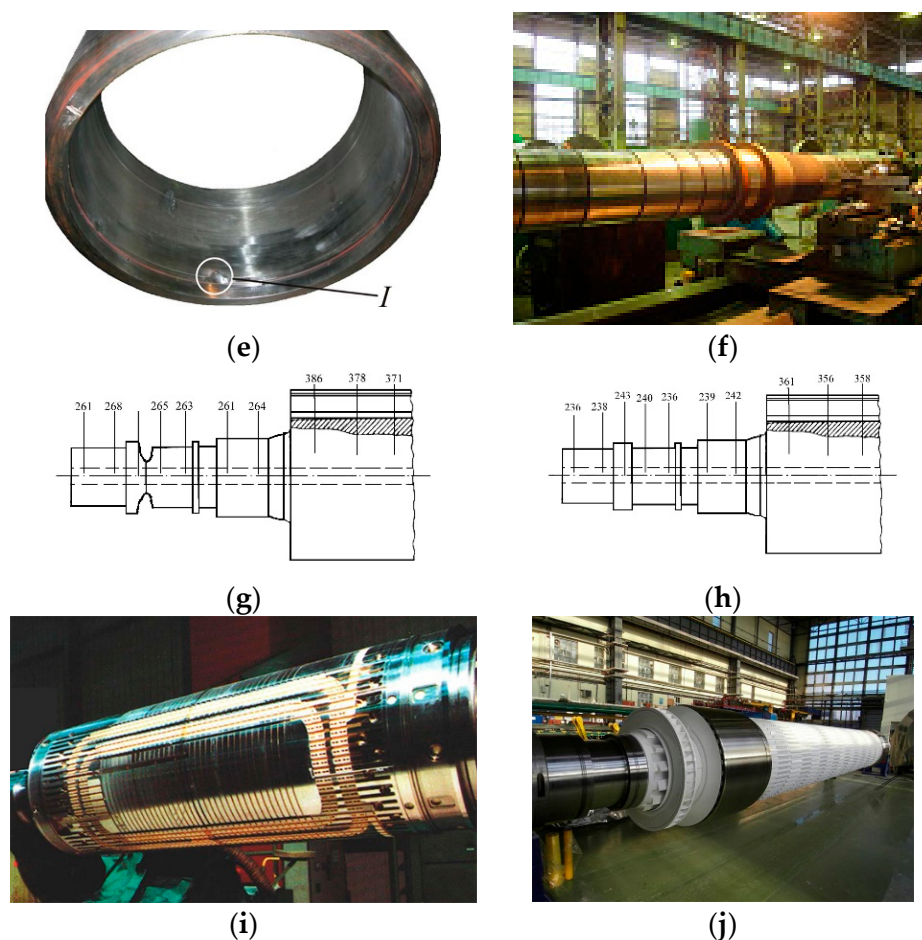(b)

(c)

(d)

Figure 18. *Cont.*

Figure 18. Part of the technological process of removing the rotor from a turbogenerator (**a**,**b**), a damaged turbogenerator rotor (**c**), the damaged outer (**d**) and inner (**e**) surfaces of a retaining ring, LCL applied in the TA during repair (**e**) with increased hardness (**g**,**h**), and the assembly of hydrogen-cooling channels (**i**) and the retaining ring after repair (**j**) [41,82,84,142,144].

In addition, knowledge about the regulations and standards, as well as the risks, associated with the operation of hydrogen devices for hydrogen-cooled TAs should enable the safe launch of TG hydrogen-cooling systems and their further operation. The most important documents on this subject are the European directives ADR-2019 (concerning the conditions for the safe transport of hydrogen), ATEX-2014 (concerning threats in areas affected by hydrogen fires and hydrogen explosions and safe distances from objects), and PED-2014 (concerning the operation of tanks and their pressure), based on which the efficiency and safety of TG hydrogen-cooling system infrastructure can be improved [125–176].

Many countries in the European Economic Area require pressure equipment manufacturers selling their products in their territory to comply with the requirements of the Pressure Equipment Directive (PED 2014/68/EU). The PED contains a set of basic requirements for pressure equipment. They relate to the pressure range and volume of the gaseous or liquid medium for which the device is designed. The PED does not instruct manufacturers how to meet these requirements but gives them the freedom to achieve compliance through a number of different production standards. All equipment subject to the PED is assigned to one or more risk categories. After determining which category the equipment belongs to, it is assigned the appropriate conformity assessment module or modules, which define the level of quality assurance and the degree of third party involvement, including: product inspection, testing, and certification; material approval; design study; type examination; approval of the quality system; approval of personnel and procedures; and approval of NDT qualifications of personnel.

Over the past 40 years, more than 100 incidents have been recorded among hydrogen energy companies, including 30 hydrogen fires, hydrogen explosions, and fire explosions that resulted in casualties. The equipment failures that were accompanied by hydrogen leakage were as follows: leakage through the flange connections of the fittings and the pipeline with hydrogen pressure tanks (up to 20%); squeezing out from rubber gaskets (housing flanges, covers) between the seal housing and the outer casing, etc., including hydrogen ignition (up to 20%); breakdown through the float's hydraulic seal (e.g., ignition in the bearing drain pipes) (up to 10%); self-ignition and leakage of hydrogen at the sharp opening of the valve at the refueling station (up to 10%); leakage through the sealing of rubber gaskets and leakage from or cracks in the bearing housing (including due to damage to the sealing insert) (up to 9%); leakage through the tanks under hydrogen pressure and the welded joints of pipelines (up to 6%); and leakage through the horizontal joints of the end shields (up to 3%). The rate of hydrogen leakage that was accompanied by ignition or "clapping" of hydrogen was approximately 15%.

Examples of hydrogen explosions that may have been of external origin include Fukushima-1, Japan, 1100 MW, 2011; Muehleberg, Switzerland, 355 MW, 1971; Fort St. Vrain, USA, 160 MW, 1987; Ignalina, Lithuania, 1988; Maine Yankee, USA, 900 MW, 1991; Brunsbuettel, Germany, 806 MW, 2001; Hamaoka-1, Japan, 540 MW, 2001; Seabrook-1, USA, 1200 MW, 2003; Yankee 1, USA, 530 MW, 2004; Cattenom-2, France, 1360 MW, 2004; etc. [117–144].

In accordance with the requirements of Directive 2014/34/EU (ATEX), manufacturers are fully responsible for the compliance of hydrogen installation products. This applies to both products manufactured individually and for private use. The technical solutions implemented by manufacturers are subject to the safety requirements contained in Directive 2014/34/EU and harmonized standards pertaining to their design and the mandatory assessment of compliance with regard to the essential safety and construction of devices intended for use in potentially explosive atmospheres.

This applies to all explosion-proof products, including non-electrical (hydrogen) equipment, electrical equipment, safety devices, components (formerly parts and subassemblies), regulation and control devices, and protective systems. Protective systems and equipment used in potentially explosive hydrogen atmospheres must be properly designed.

One of the implementations of the device-assessment process in the field of safety measure selection and one of the main streams of activity in the field of technical safety is the preparation of product documentation and the carrying out of the necessary analyses. A detailed analysis of compliance with the requirements of directives and documentation is carried out and includes completeness assessment, consultations on the selection of appropriate safety measures in potentially explosive atmospheres (EX), ignition risk assessment for non-electrical devices, necessary tests, product certification (ATEX), and full assessment of the internal control system in the production process.

The explosion at the Muskingum power plant highlights the importance of the safe design and construction of equipment and the proper management of hydrogen to prevent loss of life and property in power plants. During the explosion, the hydrogen pumping device failed, which allowed the hydrogen content in the tank to decrease and ignite. Hydrogen is used at Muskingum (and at other power stations) to cool the generator block.

Hydrogen is no more or less hazardous than other combustible materials, including natural gas and gasoline (according to the Hydrogen Safety Fact Sheet jointly published by the Hydrogen Association and the Office of the US Department of Energy Efficiency and Renewable Energy).

In fact, some of the differences specific to hydrogen provide safety benefits compared to gasoline or other fuels. However, all combustible materials must be handled responsibly. As with natural gas and petrol, hydrogen is highly flammable and can be dangerous under certain conditions. However, hydrogen can be safely handled when simple rules are followed and the user understands its characteristics [20,21,83–86,110–132].

Comparing hydrogen with other flammable materials, it is lighter than air and diffuses quickly—3.8 times faster than natural gas—which means that when it is released, it is quickly diluted to a non-flammable concentration.

Hydrogen rises at a speed of nearly 70 km/h, which is twice as fast as helium and six times faster than natural gas. Therefore, if a roof, poorly ventilated room, or other structure is trapping floating gas, the laws of physics prevent hydrogen from stagnating in the vicinity of the leak (or in the vicinity of people using hydrogen-filled equipment). Simply put, for a fire to occur, hydrogen must first be collected at a high concentration, but since hydrogen is the lightest element in the universe, it is very difficult for this to happen. Hydrogen structures help it to float up and away from the user in the event of an unexpected release.

Hydrogen is odorless, colorless, and tasteless, so human senses cannot detect any leakage. However, given the tendency for hydrogen to float rapidly, indoor hydrogen leaks briefly accumulate under the ceiling and eventually travel to corners. Due to this and other reasons, the industry often uses hydrogen sensors to detect hydrogen leaks and has maintained a high level of safety for decades. During combustion, hydrogen primarily produces heat and water. Due to the lack of carbon and the presence of heat-absorbing water vapor formed during the combustion of hydrogen, a hydrogen fire involves much less thermal radiation compared to a hydrocarbon fire.

Since hydrogen fires radiate heat near the fire (the flames themselves are just as hot), the risk of secondary fires is lower. As with any flammable substance, hydrogen can burn. However, hydrogen displacement, along with its diffusion coefficient and small molecular size, makes it difficult for it to concentrate and create a combustible situation. For a hydrogen fire to occur, the appropriate concentration of hydrogen, an ignition source, and an appropriate amount of oxidant (e.g., oxygen) must be present.

Hydrogen has a wide flammability range (4% to 74% in air) and the energy required to ignite hydrogen (0.02 MJ) can be very low. However, at low concentrations (below 10%), the energy required to ignite hydrogen is high—analogous to the energy required to ignite natural gas and gasoline in the respective flammability ranges. Hydrogen is, in fact, difficult to ignite at concentrations close to its lower flammability limit.

An explosion cannot occur in any enclosed space or container containing only hydrogen atoms. An oxidizing agent, such as oxygen, must be present at a concentration of 21% for air (volume fraction) or at least 10% for pure oxygen. Hydrogen can be explosive at concentrations from 18.3% to 59%. While this range is wide, gasoline can be more dangerous than hydrogen, as there is a risk of gasoline exploding at much lower concentrations: 1.1% to 3.3%. It is also very unlikely that hydrogen will escape from a container due to its tendency to volatilize rapidly. This is the opposite of what we see with heavier gases, such as gasoline or propane fumes, which float near the surface of the earth, creating an even greater risk of explosion.

With the exception of oxygen, any gas can cause suffocation. In most cases, buoyancy and hydrogen diffusion are unlikely to be restricted in situations where asphyxiation can occur.

Hydrogen is completely non-toxic. It does not pollute groundwater (it is a gas under normal atmospheric conditions) or the atmosphere when released. Hydrogen does not form "steam" ("vapor").

Following the power plant accidents, hydrogen supplies have been limited to delivery of only 2100 psi of hydrogen to sites (compared to the typical 2400 psi), and manufacturers' employees are now supervised by AEP personnel using a special procedure that assesses safety at work. AEP has also made other changes to the operation of the plant to ensure there are no more hazardous incidents on site. Relief valve systems are used. Hydrogen cylinders have been moved away from the space occupied by people, and the structure is protected against sources of ignition and vehicle entry.

A working group from the International Council on Large Electric Systems (CIGRE) estimated that more than 40,000 hydrogen-cooled turbogenerators could be in operation

worldwide. Despite the large number of systems using pressurized hydrogen to cool generators, most experience few incidents or problems. Given the inherently hazardous properties of hydrogen, plant personnel working with this combustible material must regularly check both the equipment and handling procedures to ensure that there are no problems [110–175].

Modern hydrogen tanks designed and manufactured in accordance with previous editions of standards and regulations for gas tanks for motor vehicles, which were approved at the time the vehicles were homologated, can still be used when the gas fuel storage systems are tight and show no signs of external damage that may affect their security. If the hydrogen storage systems are not tight, are overfilled, or have suffered damage that might affect their safety, they should, in accordance with the ADR, only be used in emergency pressure receptacles. If a hydrogen fuel storage system is equipped with two or more valves arranged in series, the two valves should be closed so as to be tight under normal conditions of carriage. If only one valve is functioning properly, all openings, with the exception of the pressure relief device, should be closed so as to be tight under normal conditions of carriage. Hydrogen gas fuel storage systems should be transported in such a way that they are protected against the jamming of the pressure relief device, against any damage to valves or other pressurized parts of the gas supply, and against accidental release of gas under normal conditions of carriage. Gas fuel storage systems should be secured against shifting or vertical displacement.

In order to make modern gas fire suppression systems more widely applicable, further research is needed in future work. Only small cracks were considered in this study. If doors or windows are open, the size of the opening can significantly affect the flow of the air–aggregate mixture. It should also be taken into account that a permanent ignition source can cause a renewed fire if fresh air can enter the enclosure through openings or cracks. Computer neural networks and artificial intelligence systems, such as Generative Pre-Trained Transformer 3 (GPT-3), could be used in further research.

6. Conclusions

It was established that corrosion protection through the application of fire-resistant LCLs resulted in increases in tool life when turning and drilling 38KHN3MFA steel by ~1.6 times and by 60%, respectively.

Evaluation using the appearance of chips as an "indicator" after 100 h following turning confirmed the reliability of the postoperative protective effect of LCL against corrosion.

When using water and LCL, physical and chemical destruction processes occur that affect the morphology of the chips. The chips become more compact and acquire a rounded shape. Since ferrite belongs to the plastic phase and pearlite to the brittle phase, the adjustment of the structural-phase alloy affects the amounts of brittle or ductile fracturing.

After the use of water and LCL, the concentration of hydrogen in the cutting products of 38KHN3MFA steel increased, which indicated its participation in facilitating destruction during machining. In the chips formed when using LCL, the amount of hydrogen increased by 2.25 times compared to the chips obtained with the dry treatment, while treatment with coolants resulted in an increase of 2.6 times, indicating an intense flow of decomposition products of LCL through diffusion processes in the cutting zone. Hydrogen reduces energy costs for the destruction of structural and phase components and promotes their dispersion.

The creation of 2D and 3D images allowed for a more detailed approach to the study of the influence of LCL on surface treatment. In order to make modern approaches to increasing turbine-hall fire safety using suppression systems more widely applicable, computer neural networks and artificial intelligence systems, such as Generative Pre-trained Transformer 3 (GPT-3), can be used.

Individually, the author contributions were as follows: conceptualization, A.I.B., M.R.H. and L.M.I.; data curation, A.I.B., M.R.H., V.O.B. and V.O.K.; formal analysis, A.I.B., L.M.I., M.R.H., V.O.B. and V.O.K.; investigation, L.M.I., V.O.K., V.O.B. and M.R.H.; methodology, A.I.B., M.R.H., V.O.B., V.O.K. and L.M.I.; writing—original draft, A.I.B.; writing—review and editing, A.I.B. and L.M.I.; software, V.O.K.; validation, A.I.B., M.R.H., V.O.B. and L.M.I.; resources, L.M.I.; A.I.B. and V.O.K.; visualization, V.O.B. and V.O.K.; supervision, A.I.B.; project administration, A.I.B.; funding acquisition, A.I.B. All authors have read and agreed to the published version of the manuscript.

Abbreviations

LCL	lubricating cooling liquid
LCL_o	lubricating cooling liquid based on petroleum oil
LCL_s	lubricating cooling liquid based on sunflower oils
LCL_r	lubricating cooling liquid based on rapeseed oils
σ_u	ultimate tensile strength (UTS)
$\sigma_{0,2}$	yield strength (YS)
δ	elongation
ψ	reduction in area
C_H	hydrogen concentration
ppm	parts per million
RPM	rotations per minute
TA	turboaggregate (turbine + turbogenerator)
TG	hydrogen-cooling turbogenerator

References

1. Lawal, S.A.; Choudary, I.A.; Nukman, Y. Application of vegetable oil-based metal working fluids in machining ferrous metals. A review. *Int. J. Mach. Tools Manuf.* **2012**, *52*, 1–12. [CrossRef]
2. Koushik, A.V.; Shetty, S.N.; Ramprasad, C. Vegetable Oil-Based Metal Working Fluids. A Review. *Int. J. Theor. Appl. Res. Mech. Eng. IJTARME* **2012**, *1*, 95–101. [CrossRef]
3. Nagendramma, P.; Kaul, S. Development of eco-friendly/biodegradable lubricants: An overview. *Renew. Sustain. Energy Rev.* **2012**, *16*, 764–774. [CrossRef]
4. Shashidhara, Y.M.; Jayaram, S.R. Vegetable oils as a potential cutting fluid. An evolution. *Tribol. Int.* **2010**, *43*, 1073–1108. [CrossRef]
5. Doll, K.M.; Sharma, B.K. Emulsification of Chemically Modified Vegetable Oils for Lubricant Use. *J. Surfactants Deterg.* **2011**, *14*, 131–138. [CrossRef]
6. Seung-Hyun, Y.; Young-Wun, K.; Kunwoo, C.; Seung-Yeop, B.; Joon-Seop, K. Synthesis and corrosion inhibition behavior of imidazoline derivatives based on vegetable oil. *Corros. Sci.* **2012**, *59*, 42–54. [CrossRef]
7. Jacob, J.; Mrinal, B.; Peter, C.R. Emulsions containing vegetable oils for cutting fluid application. *Colloids Surf. Physicochem. Eng. Aspects* **2004**, *237*, 141–150. [CrossRef]
8. Sokovic, M.; Mijanovic, K. Ecological aspects of the cutting fluids and its influence on the quantifiable parameters of the cutting processes. *J. Mater. Process. Technol.* **2001**, *109*, 181–189. [CrossRef]
9. Stupnytskyy, V.; Hrytsay, I. Comprehensive analysis of the product's operational properties formation considering machining technology. *Arch. Mech. Eng.* **2020**, *67*, 149–167. [CrossRef]
10. Kuram, E.; Ozcelik, B.; Simsek, B.T.; Demirbas, E. The effect of extreme pressure added vegetable based cutting fluids on cutting performance in milling. *Ind. Lubr. Tribol.* **2013**, *65*, 181–193. [CrossRef]
11. Buczek, B.; Zajezierska, A. Biodegradable lubricating greases containing used frying oil as additives. *Ind. Lubr. Tribol.* **2015**, *67*, 315–319. [CrossRef]

12. Nagendramma, P. Alternative Industrial Biolubricants: Possible Future for Lubrication. In *Book Industrial Tribology*; CRC Press: Boca Raton, FL, USA, 2022; p. 22, ISBN 9781003243205. Available online: https://www.taylorfrancis.com/chapters/edit/10.1201/9781003243205-4/alternative-industrial-biolubricants-ponnekanti-nagendramma (accessed on 27 November 2022).

13. Ahmad, M.A.; Suadi, S.H.; Rahman, N.A. Palm oil ester properties as lubricant base oil. *Proc. Mech. Eng. Res. Day* **2022**, *8*, 263–264. Available online: https://www3.utem.edu.my/care/proceedings/merd22/pdf/10%20Surface%20Engineering%20and%20Tribology/124_p263_264.pdf (accessed on 27 November 2022).

14. Juwita, M.; Faizal, M.; Said, M.; Prianto, J.; Hartawan, R.A.; Aprianti, N. Synthesis of Crude Palm Oil-Based Polyol Ester as Biolubricant. *Rekayasa J. Penerapan Teknol. Dan Pembelajaran* **2021**, *19*, 62–74. [CrossRef]

15. Xavior, M.A.; Adithan, M. Determining the influence of cutting fluids on tool wear and surface roughness during turning of AISI 304 austenitic stainless steel. *J. Mater. Process. Technol.* **2009**, *20*, 900–909. [CrossRef]

16. Belluco, W.; De Chiffre, L. Performance evaluation of vegetable-based oils in drilling austenitic stainless steel. *J. Mater. Process. Technol.* **2004**, *148*, 171–176. [CrossRef]

17. Ahmad, U.; Naqvi, S.R.; Ali, I.; Naqvi, M.; Asif, S.; Bokhari, A.; Juchelková, D.; Klemeš, J.J. A review on properties, challenges and commercial aspects of eco-friendly biolubricants productions. *Chemosphere* **2022**, *1*, 309. [CrossRef]

18. MohdNor, N.; Salih, N.; Salimon, J. Optimization and lubrication properties of Malaysian crude palm oil fatty acids based neopentyl glycol diester green biolubricant. *Renew. Energy* **2022**, *200*, 942–956. [CrossRef]

19. Pawar, R.V.; Hulwan, D.B.; Mandale, M.B. Recent advancements in synthesis, rheological characterization, and tribological performance of vegetable oil-based lubricants enhanced with nanoparticles for sustainable lubrication. *J. Clean. Prod.* **2022**, *378*, 134454. [CrossRef]

20. Balitskii, A.; Kolesnikov, V.; Abramek, K.F.; Balitskii, O.; Eliasz, J.; Marya, H.; Ivaskevych, L.; Kolesnikova, I. Influence of hydrogen-containing fuels and environmentally friendly lubricating coolant on nitrogen steels wear resistance for spark ignition engine pistons and rings kit gasket set. *Energies* **2021**, *14*, 7583. [CrossRef]

21. Balitskii, O.A.; Kolesnikov, V.O.; Balitskii, A.I.; Eliasz, J.J.; Havryliuk, M.R. Hydrogen effect on the high-nickel surface steel properties during machining and wear with lubricants. *Arch. Mater. Sci. Eng.* **2020**, *104*, 49–57. [CrossRef]

22. Balyts'kyi, O.I.; Kolesnikov, V.O.; Havrylyuk, M.R. Influence of modification of 38KhN3MFA steel on the structural-phase state and cutting products under variable technological conditions. *Mater. Sci.* **2020**, *55*, 915–920. [CrossRef]

23. Balyts'kyi, O.I.; Kolesnikov, V.O.; Havrylyuk, M.R. Influence of lubricating liquid on the formation of the products of cutting of 38KhN3MFA Steel. *Mater. Sci.* **2019**, *54*, 722–727. [CrossRef]

24. Che Sidik, N.A.C.; Yazid, M.N.A.W.M.; Mamat, R. A review on the application of nanofluids in vehicle engine cooling system. *Int. Commun. Heat Mass Transf.* **2015**, *68*, 85–90. [CrossRef]

25. Kodali, D.R. High performance ester lubricants from natural oils. *Ind. Lubr. Tribol.* **2002**, *54*, 165–170. [CrossRef]

26. Balitskii, O.; Kolesnikov, V. Identification of Wear Products in the Automotive Tribotechnical System Using Computer Vision Methods, Artificial Intelligence and Big Data. In Proceedings of the 2019 XIth International Scientific and Practical Conference on Electronics and Information Technologies (ELIT), Lviv, Ukraine, 16–18 September 2019; pp. 24–27. Available online: https://ieeexplore.ieee.org/document/8892275 (accessed on 27 November 2022). [CrossRef]

27. Balitskii, O.I.; Havryliuk, M.R.; Deviatkin, R.M.; Fedusiv, I.R. Application of modified sun flower oil as emulsifier of lubricating-cooling liquids. *Mater. Sci.* **2013**, *49*, 382–385. [CrossRef]

28. Gwyddion. Available online: http://gwyddion.net/presentations/tutorials.php (accessed on 27 November 2022).

29. Rueden, C.T.; Schindelin, J.; Hiner, M.C.; DeZonia, B.E.; Walter, A.E.; Arena, E.T.; Eliceiri, K.W. ImageJ2: ImageJ for the next generation of scientific image data. *BMC Bioinform.* **2017**, *18*, 529. [CrossRef]

30. Balitskii, A.; Hawrilyuk, M.; Eliasz, J.; Balitska, W.; Kolesnikow, W. Efektywnosc olejow roslinnych jako cieczy smarujaco-chlodzacych w obrobce skrawaniem stali wirnikowych. *Mechanik* **2015**, *8–9*, 168–176. Available online: https://www.mechanik.media.pl/artykuly/efektywnosc-olejow-roslinnych-jako-cieczy-smarujaco-chlodzacych-w-obrobce-skrawaniem-stali-wirnikowych.html (accessed on 27 November 2022).

31. Kindrachuk, M.; Volchenko, D.; Balitskii, A.; Abramek, K.F.; Volchenko, M.; Balitskii, O.; Skrypnyk, V.; Zhuravlev, D.; Yurchuk, A.; Kolesnikov, V. Wear resistance of spark ignition engine piston rings in hydrogen-containing environments. *Energies* **2021**, *14*, 4801. [CrossRef]

32. Balyts'kyi, O.I.; Kolesnikov, V.O. Investigation of the wear products of austenitic manganese cast irons. *Mater. Sci.* **2004**, *40*, 78–82. [CrossRef]

33. Balyts'kyi, O.I.; Kolesnikov, V.O.; Eliasz, Y.; Havrylyuk, M.R. Specific features of the fracture of hydrogenated high-nitrogen manganese steels under conditions of rolling friction. *Mater. Sci.* **2015**, *50*, 604–611. [CrossRef]

34. Zhao, F.; Clarens, A.; Murphree, A.; Hayes, K.; Skerlos, S.J. Structural Aspects of Surfactant Selection for the Design of Vegetable Oil Semi-Synthetic Metalworking Fluids. *Environ. Sci. Technol.* **2006**, *40*, 7930–7937. [CrossRef]

35. Chinwuba, V.O.; Hung, G.H.; Hosung, K. Tribological evaluation of selected biodegradable oils with long chain fatty acids. *Ind. Lubr. Tribol.* **2010**, *62*, 26–31. [CrossRef]

36. Maleque, M.A.; Masjuki, H.H.; Sapuan, S.M. Vegetable-based biodegradable lubricating oil additives. *Ind. Lubr. Tribol.* **2003**, *55*, 137–143. [CrossRef]

37. Bartz, W.J. Lubricants and the environment. *Tribol. Int.* **1998**, *31*, 35–47. [CrossRef]

38. Balyts'kýi, O.I.; Havrylyuk, M.R.; Kochubei, V.V.; Elias, Y. Influence of the thermal resistance of liquid coolants on the machining of 12Kh18AG18SH steel. *Mater. Sci.* **2016**, *52*, 200–208. [CrossRef]

39. Balitskii, A.; Hawrilyuk, M.; Eliasz, J.; Balitska, W.; Kolesnikow, W. Oddziaływanie wodoru na kształtowanie i odprowadzenie wiórów w obróbce skrawaniem stali wysokostopowych z użyciem ekologicznych cieczy smarująco-chłodzących. *Mechanik* **2016**, *10*, 1412–1413. Available online: https://www.mechanik.media.pl/artykuly/oddzialywanie-wodoru-na-ksztaltowanie-i-odprowadzenie-wiorow-w-obrobce-skrawaniem-stali-wysokostopowych-z-uzyciem-ekologicznych-cieczy-smarujaco-chlodzacych.html (accessed on 27 November 2022). [CrossRef]

40. Balitskii, A.; Eliasz, J.; Balitska, W.; Kochubei, W.; Hawrilyuk, M. Wplyw wytrzymalosci termicznej cieczy smarujaco-chlodzacych na ich zdolnosc do pracy w warunkach skrawania. *Mechanik Nowatorskie Rozw. Obrobki Otworow.* **2014**, *8–9*, 733. Available online: http://www.mechanik.media.pl/archiwum,szukaj;2014,0,0.html (accessed on 27 November 2022).

41. Balitskii, A.; Krohmalny, O.; Ripey, I. Hydrogen cooling of turbogenerators and the problem of rotor retaining ring materials degradation. *Int. J. Hydrogen Energy* **2000**, *25*, 167–171. [CrossRef]

42. Balitski, A.; Hawrilyuk, M.; Balitska, W.; Kowalenko, W. Wplyw cieczy smarujaco-chlodzacych na proces wiercenia stali wysokoazotowej. *Mechanik* **2013**, *8–9*, 712–716. Available online: https://www.mechanik.media.pl/archiwum,szukaj;2013,0,0.html (accessed on 27 November 2022).

43. Balyts'kyi, O.I.; Kolesnikov, V.O.; Kubicki, E. Enhancement of the crack resistance of manganese cast irons. *Mater. Sci.* **2005**, *41*, 67–73. [CrossRef]

44. Balitskii, O.A.; Kolesnikov, V.O.; Balitskii, A.I. Wear resistance of hydrogenated high nitrogen steel at dry and solid state lubricants assistant friction. *Arch. Mater. Sci. Eng.* **2019**, *98*, 57–67. [CrossRef]

45. Balitskii, A.; Kindrachuk, M.; Volchenko, D.; Abramek, K.F.; Balitskii, O.; Skrypnyk, V.; Zhuravlev, D.; Bekish, I.; Ostashuk, M.; Kolesnikov, V. Hydrogen containing nanofluids in the spark engine's cylinder head cooling system. *Energies* **2022**, *15*, 59. [CrossRef]

46. Balitskii, A.A.; Kolesnikov, V.A.; Vus, O.B. Tribotechnical properties of nitrogen manganese steels under rolling friction at addition of $(GaSe)_xIn_{1-x}$, powders into contact zone. *Metallofiz. Noveishie Tekhnologii.* **2010**, *32*, 685–695. Available online: https://www.scopus.com/record/display.uri?eid=2-s2.0-77957864676&origin=resultslist&sort=plf-f#metrics (accessed on 27 November 2022).

47. Balyts'kyi, O.I.; Kolesnikov, V.O. Investigation of wear products of high-nitrogen manganese steels. *Mater. Sci.* **2009**, *45*, 576–581. [CrossRef]

48. Balyts'kyi, O.I.; Kolesnikov, V.O.; Kawiak, P. Triboengineering properties of austenitic manganese steels and cast irons under the conditions of sliding friction. *Mater. Sci.* **2005**, *41*, 624–630. [CrossRef]

49. Balitskii, A.; Kolesnikov, V. Hydrogen Effects on the Formation of Nickel Based Superalloys Cutting and Wear Products. In Proceedings of the 22nd European Conference on Fracture-ECF22, Belgrade, Serbia, 26–31 August 2018; p. 182, ISBN 978-86-900686-0-9. Available online: http://www.ecf22.rs/docs/Book%20of%20Abstracts%20ECF22.pdf (accessed on 27 November 2022).

50. Osenin, Y.I.; Krivosheya, D.S.; Krivosheya, Y.V. Disc Brake with two thermally insulated friction units with different frictional properties. *J. Frict. Wear* **2022**, *43*, 124–127. [CrossRef]

51. Beleggia, M.; Lau, J.W.; Schofield, M.A.; Zhu, Y.; Tandon, S.; De Graef, M. Phase diagram for magnetic nano-rings. *J. Magn. Magn. Mater.* **2006**, *301*, 131–146. [CrossRef]

52. Jha, D.; Singh, S.; Al-Bahrani, R.; Liao, W.; Choudhary, A.; De Graef, M.; Agrawal, A. Extracting grain orientations from EBSD patterns of polycrystalline materials using convolutional neural networks. *Microsc. Microanal.* **2018**, *24*, 497–502. [CrossRef]

53. Tandon, S.; Beleggia, M.; Zhu, Y.; De Graef, M. On the computation of the demagnetization tensor for uniformly magnetized particles of arbitrary shape. Part II: Numerical approach. *J. Magn. Magn. Mater.* **2004**, *271*, 27–38. [CrossRef]

54. Singh, S.; De Graef, M. Dictionary Indexing of Electron Channeling Patterns. *Microsc. Microanal.* **2017**, *23*, 1–10. [CrossRef] [PubMed]

55. Biery, N.E.; De Graef, M.; Pollock, T.M. Influence of microstructure and strain distribution on failure properties in intermetallic TiAl-based alloys. *Mater. Sci. Eng. A* **2001**, *319–321*, 613–617. [CrossRef]

56. Vronka, M.; Straka, L.; De Graef, M.; Heczko, O. Antiphase boundaries, magnetic domains, and magnetic vortices in Ni–Mn–Ga single crystals. *Acta Mater.* **2020**, *184*, 179–186. [CrossRef]

57. Chesser, I.; Francis, T.; De Graef, M.; Holm, E.A. Learning the grain boundary manifold: Tools for visualizing and fitting grain boundary properties. *Acta Mater.* **2020**, *195*, 209–218. [CrossRef]

58. Huffman, L.; Simmons, J.; De Graef, M.; Pollak, I. Shape priors for MAP segmentation of alloy micrographs using graph cuts. In Proceedings of the 2011 IEEE Statistical Signal Processing Workshop (SSP), Nice, France, 28–30 June 2011; pp. 661–664. [CrossRef]

59. Charpagne, M.A.; Polonsky, A.T.; Echlin, M.P.; Jacomet, S.; De Jaeger, J.; De Graef, M.; Bozzolo, N.; Pollock, T.M. Growth accidents induced by primary γ' precipitates in a polycrystalline nickel-based superalloy. *Scr. Mater.* **2020**, *186*, 109–113. [CrossRef]

60. Ulutan, D.; Ozel, T. Machining induced surface integrity in titanium and nickel alloys: a review. *Int. J. Mach. Tools Manuf.* **2011**, *250*, 280. [CrossRef]

61. Kaya, E.; Qingan Yin, Y.C.; Akyüz, B.; Liu, Z.; Wang, B.; Song, Q.; Cai, Y. Effects of cutting parameters on machinability characteristics of Ni-based superalloys: A review. *Gruyter Open Access Open Eng.* **2017**, *7*, 37. [CrossRef]

62. Yin, Q.; Liu, Z.; Wang, B.; Song, Q.; Cai, Y. Recent progress of machinability and surface integrity for mechanical machining Inconel 718: A review. *Int. J. Adv. Manuf. Technol.* **2020**, *109*, 215–245. [CrossRef]

63. Bordina, A.; Bruschia, S.; Ghiottia, A. The effect of cutting speed and feed rate on the surface integrity in dry turning of CoCrMo alloy. 2nd CIRP Conference on Surface Integrity (CSI). *Procedia CIRP* **2014**, *13*, 219–224. [CrossRef]

64. Isik, Y. Using internally cooled cutting tools in the machining of difficult-to-cut materials based on Waspaloy. *Adv. Mech. Eng.* **2016**, *8*, 16878140166478. [CrossRef]

65. Olufayo, O.A.; Che, H.; Songmene, V.; Katsari, C.; Yue, S. Machinability of Rene 65 Superalloy. *Materials* **2019**, *12*, 2034. [CrossRef]

66. Fan, W.; Ji, W.; Wang, L.; Zheng, L.; Wang, Y. A review on cutting tool technology in machining of Ni-based Superalloys. *Int. J. Adv. Manuf. Technol.* **2020**, *110*, 2863–2879. [CrossRef]

67. Glotka, A.A.; Haiduk, S.V.; Ol'shanetskii, V.Y. Modeling Thermophysical Characteristics of Nickel-Based Superalloys. *J. Eng. Phys. Thermophys.* **2021**, *94*, 1363–1368. [CrossRef]

68. Ol'shanetskii, V.E.; Glotka, A.A. Distribution of elements within carbides of multicomponent alloys of the Ni–Cr–Co–Al–W–Re–Ta–Mo–Nb–C system. *Met. Sci. Heat Treat.* **2021**, *63*, 318–326. [CrossRef]

69. Glotka, O.A. Distribution of alloying elements in carbides of refractory nickel alloys under the conditions of equiaxial crystallization. *Mater. Sci.* **2021**, *56*, 714–721. [CrossRef]

70. Glotka, O.A.; Gayduk, S.V.; Olshanetskiy, V.Y. The distribution of alloying elements in secondary carbides of heat-resistant nickel alloys. *Metalozn. Obrobka Met.* **2020**, *26*, 25–36. [CrossRef]

71. Dmytrakh, I.M.; Akid, R.; Miller, K.J. Electrochemistry of deformed smooth surfaces and short corrosion fatigue crack growth behaviour. *Br. Corros. J.* **1997**, *32*, 138–144. [CrossRef]

72. Syrotyuk, A.M.; Dmytrakh, I.M. Methods for the evaluation of fracture and strength of pipeline steels and structures under the action of working media. Part I. Influence of the corrosion factor. *Mater. Sci.* **2014**, *50*, 324–339. [CrossRef]

73. Balitskii, O.; Borowiak-Palen, E.; Konicki, W. Synthesis and characterization of colloidal gallium selenide nanowires. *Cryst. Res. Technol.* **2011**, *46*, 417–420. [CrossRef]

74. Akid, R.; Dmytrakh, I.M.; Gonzalez-Sanchez, J. Fatigue damage accumulation: The role of corrosion on the early stages of crack development. *Corros. Eng. Sci. Technol.* **2006**, *41*, 328–335. [CrossRef]

75. Bihun, R.I.; Stasyuk, Z.V.; Balitskii, O.A. Crossover from quantum to classical electron transport in ultrathin metal films. *Phys. B Condens. Matter* **2016**, *487*, 73–77. [CrossRef]

76. Capelle, J.; Dmytrakh, I.; Gilgert, J.; Jodin, P.; Pluvinage, G. A comparison of experimental results and computations for ctacked tubes subjected to internal pressure. *Mater. Tehnol.* **2006**, *40*, 233–237. Available online: http://mit.imt.si/izvodi/mit066/capelle.pdf (accessed on 27 November 2022).

77. Benghalia, M.A.; Faces, C.; Khadrauui, A.; Meliani, M.H.; Obot, I.B.; Sorrour, A.; Dmytrakh, M.; Azari, Z. Performance evaluation of a natural and synthetic compound as corrosion inhibitors of API 5l X52 steel in hydrochloric acid media. *Moroc. J. Chem.* **2018**, *6*, 51–61. [CrossRef]

78. Balitskii, O.A.; Savchyn, V.P.; Savchyn, P.V. Thermal oxidation of indium and gallium sulphides. *Phys. B Condens. Matter* **2005**, *355*, 365–369. [CrossRef]

79. Aksimentyeva, O.I.; Demchenko, P.Y.; Savchyn, V.P.; Balitskii, O.A. The chemical exfoliation phenomena in layered GaSe-polyaniline composite. *Nanoscale Res. Lett.* **2013**, *8*, 29. [CrossRef] [PubMed]

80. Rozumek, D.; Macha, E. Elastic-plastic fatigue crack growth in 18G2A steel under proportional bending with torsion loading. *Fatigue Fract. Eng. Mater. Struct.* **2006**, *29*, 135–145. [CrossRef]

81. Moustabchir, H.; Azari, Z.; Hairi, S.; Dmytrakh, I. Experimental and computed stress distribution ahead of notch in pressure vessel: Application of T-stress conception. *Comput. Mater. Sci.* **2012**, *58*, 59–66. [CrossRef]

82. Balitskii, A.I.; Ivaskevich, L.M.; Balitskii, O.A. Rotor steels crack resistance and fracture behavior for hydrogen targeted materials ever-widening database. *Eng. Fract. Mech.* **2022**, *260*, 108168. [CrossRef]

83. Panasyuk, V.V.; Dmytrakh, I.M.; Toth, L.; Bilyi, O.L.; Syrotyuk, A.M. A method for the assessment of the serviceability and fracture hazard for structural elements with cracklike defects. *Mater. Sci.* **2014**, *49*, 565–576. [CrossRef]

84. Balitskii, A.I.; Dmytryk, V.V.; Ivaskevich, L.M.; Balitskii, O.A.; Glushko, A.V.; Medovar, L.B.; Abramek, K.F.; Stovpchenko, G.P.; Eliasz, J.J.; Krolikowski, M.A. Improvement of the Mechanical Characteristics, Hydrogen Crack Resistance and Durability of Turbine Rotor Steels Welded Joints. *Energies* **2022**, *15*, 6006. [CrossRef]

85. Balitskii, A.; Ivaskevich, L.; Mochulskyi, V.; Eliasz, J.; Skolozdra, O. Influence of high pressure and high temperature hydrogen on fracture toughness of Ni-containing steels and alloys. *Arch. Mech. Eng.* **2014**, *61*, 129–138. [CrossRef]

86. Balyts'kyi, O.I.; Chmiel, J.; Krause, P.; Niekrasz, J.; Maciag, M. Role of hydrogen in the cavitation fracture of 45 steel in lubricating media. *Mater. Sci.* **2009**, *45*, 651–654. [CrossRef]

87. Balyts'kyi, O.I.; Ivas'kevych, L.M.; Mochul's'kyi, V.M.; Holiyan, O.M. Influence of hydrogen on the crack resistance of 10Kh15N27T3V2MR steel. *Mater. Sci.* **2009**, *45*, 258–267. [CrossRef]

88. Glotka, A. Prediction thermo-physical characteristics heat-resistant nickel alloys directional crystallization. *Acta Metall. Slovaca* **2021**, *27*, 68–71. [CrossRef]

89. Balitska, V.; Filipecki, J.; Shpotyuk, O.; Swiatek, J.; Vakiv, M. Dynamic radiation-induced effects in chalcogenide vitreous compounds. *J. Non Cryst. Solids* **2001**, *287*, 216–221. [CrossRef]

90. Syrotyuk, A.M.; Dmytrakh, I.M. Methods for the evaluation of fracture and strength of pipeline steels and structures under the action of working media. Part II. Influence of hydrogen-containing media. *Mater. Sci.* **2015**, *50*, 475–487. [CrossRef]

91. Wasim, M.; Djukic, M.B.; Ngo, T.D. Influence of hydrogen-enhanced plasticity and decohesion mechanisms of hydrogen embrittlement on the fracture resistance of steel. *Eng. Fail. Anal.* **2021**, *123*, 105312. [CrossRef]

92. Hrytsay, I.; Stupnytskyy, V. Advanced computerized simulation and analysis of dynamic processes during the gear hobbing. In *Advanced Manufacturing Processes. InterPartner-2019*; Lecture Notes in Mechanical Engineering; Tonkonogyi, V., Ed.; Springer: Cham, Switzerland, 2020. [CrossRef]

93. Hrytsay, I.; Stupnytskyy, V. Analysis of the involute and sinusoidal gears by the operating parameters and a new method of its cutting. In *Advances in Design, Simulation and Manufacturing II. DSMIE 2019*; Lecture Notes in Mechanical Engineering; Ivanov, V., Trojanowska, J., Machado, J., Liaposhchenko, O., Zajac, J., Pavlenko, I., Edl, M., Perakovic, D., Eds.; Springer: Cham, Switzerland, 2020. [CrossRef]

94. Glotka, A.A.; Moroz, A.N. Comparison of the effects of carbides and nonmetallic inclusions on formation of fatigue microcracks in steels. *Met. Sci. Heat Treat.* **2019**, *61*, 521–524. [CrossRef]

95. Glotka, O.A. Modelling the composition of carbides in nickel-based superalloys of directional crystallization. *J. Achiev. Mater. Manuf. Eng.* **2020**, *102*, 5–15. [CrossRef]

96. Safety Standards for Hydrogen and Hydrogen Systems, NASA NSS 1740.16. 2005. Available online: https://www.energy.gov/sites/prod/files/2014/03/f11/871916.pdf (accessed on 27 November 2022).

97. Di Nenno, P.J.; Forssell, E.W. Clean agent total flooding fire extinguishing systems. In *SFPE Handbook of Fire Protection Engineering*, 5th ed.; Springer: New York, NY, USA, 2016; Chapter 44; ISBN 978-1-4939-2564-3. [CrossRef]

98. Beyler, C. Flammability limits of premixed and diffusion flames. In *SFPE Handbook of Fire Protection Engineering*, 5th ed.; Springer: New York, NY, USA, 2016; Chapter 17; ISBN 978-1-4939-2564-3. [CrossRef]

99. Purser, D.A. Combustion Txoicity. In *SFPE Handbook of Fire Protection Engineering*, 5th ed.; Hurley, M.J., Gottuk, D.T., Hall, J.R., Jr., Harada, K., Kuligowski, E.D., Puchovsky, M., Torero, J.L., Watts, J.M., Jr., Wieczorek, C.J., Eds.; SFPE: Gaithersburg, MD, USA, 2016; Chapter 62; pp. 2207–2307. [CrossRef]

100. Lambertsen, C.J. *Summary of Relations, Physiologic Factors and Fire Protection and Engineering Design*; Report 4-14-92; Environmental Biochemical Research Data Center (EBRDC), Institute of Environmental Medicine: Philadelphia, PA, USA; University of Pennsylvania: Philadelphia, PA, USA, 1994. Available online: https://www.facilities.upenn.edu/sites/default/files/pdfs/211300_-_fire_suppression_systems_-_fire_protection_design_guide.pdf (accessed on 27 November 2022).

101. Laursen, T. Fire protection for weak citizens. In Proceedings of the Nordic Fire and Safety Days, Copenhagen, Denmark, 20–21 August 2019; RISE Research Institutes of Sweden AB: Gothenburg, Sweden, 2019.

102. *ISO 14520-1*; Gaseous Fire Extinguish Systems–Physical Properties and System Design, Part 1: General Requirements. International Standards Organization: Geneva, Switzerland, 2006. Available online: https://www.iso.org/obp/ui/#iso:std:iso:14520:-1:ed-2:v1:en (accessed on 27 November 2022).

103. Kraaijeveld, A. Fire protection of at risk groups by IG-541 and water based sprinklers: Full scale tests. In Proceedings of the Nordic 432 Fire and Safety Days, Copenhagen, Denmark, 20–21 August 2019; RISE Research Institutes of Sweden AB: Gothenburg, Sweden, 2019. [CrossRef]

104. Fire Eater. Fire Eater Control Inert Ci Manual for UL Listed Extinguishing System. Fire Eater A/S. 2013. Available online: https://www.scribd.com/document/517403850/Fire-Eater-Control-Inert-Ci-Manual-for-U (accessed on 27 November 2022).

105. McGrattan, K.; Hostikka, S.; McDermott, R.; Floyd, J.; Weinschenk, C.; Overholt, K. Fire dynamics simulator user's guide. In *NIST Special Publication*, 6th ed.; NIST: Gaithersburg, MD, USA, 2013. [CrossRef]

106. Hu, X.; Jia, F.; Wang, Z.; Galea, E. Grouping methods for MPS soot transport model and its application in large-scale enclosure fires. *Fire Saf. J.* **2017**, *9*, 361–370. [CrossRef]

107. Hu, X. Numerical study of the effects of ventilation velocity on peak heat release rate and the confinement velocity in large tunnel fires. *Saf. Sci.* **2021**, *142*, 105359. [CrossRef]

108. McGrattan, K.; Hostikka, S.; McDermott, R.; Floyd, J.; Weinschenk, C.; Overholt, K. Fire dynamics simulator technical reference guide volume 1: Mathematical model. In *NIST Special Publication*, 6th ed.; NIST: Gaithersburg, MD, USA, 2013. [CrossRef]

109. Song, C.; Jiang, H.; Gao, W. High temperature generated by sliding metal friction and its effectiveness as an ignition source for hydrogen. *J. Loss Prev. Process Ind.* **2022**, *79*, 104833. [CrossRef]

110. Shibani, R.J.; Aryai, V. Computational fluid dynamics modelling of a hydrogen fire safety in a scaled tunnel environment. *Saf. Extrem. Environ.* **2022**, *1*, 1–15. [CrossRef]

111. Abohamzeh, E.; Salehi, F.; Sheikholeslami, M.; Abbassi, R.; Khan, F. Review of hydrogen safety during storage, transmission, and applications processes. *J. Loss Prev. Process Ind.* **2021**, *72*, 104569. [CrossRef]

112. Wei, R.; Lan, J.; Lian, L.; Huang, S.; Zhao, C.; Dong, Z.; Weng, J. A bibliometric study on research trends in hydrogen safety. *Process Saf. Environ. Prot.* **2022**, *159*, 1064–1081. [CrossRef]

113. Tang, Z.; Zhao, K.; Wang, Z.; Wang, J.; Pan, Y. Study on the extension length of horizontal hydrogen jet fires under the action of water curtain. *Fuel* **2022**, *322*, 124254. [CrossRef]

114. Wang, N.; Huang, S.; Zhang, Z.; Li, T.; Yi, P.; Wu, D.; Chen, G. Laminar burning characteristics of ammonia/hydrogen/air mixtures with laser ignition. *Int. J. Hydrogen Energy* **2021**, *46*, 31879–31893. [CrossRef]

115. Xie, Y.; Lv, N.; Huang, Y.; Wu, D.; Gong, L.; Yang, X.; Zeng, Y. Comparative analysis on temperature characteristics of hydrogen-powered and traditional fossil-fueled vehicle fires in the tunnel under longitudinal ventilations. *Int. J. Hydrogen Energy* **2022**, *47*, 24107–24118. [CrossRef]

116. Lyu, G.; Zhong, C.; Gou, X. A pressure-ratio equivalent method for ultra-high pressure hydrogen spontaneous ignition experiment. *Int. J. Hydrogen Energy* **2022**, *47*, 22650–22661. [CrossRef]

117. Zhou, S.; Luo, Z.; Wang, T.; He, M.; Li, R.; Su, B. Research progress on the self-ignition of high-pressure hydrogen discharge: A review. *Int. J. Hydrogen Energy* **2022**, *47*, 9460–9476. [CrossRef]

118. Sun, R.; Pu, L.; Yu, H.; Dai, M.; Li, Y. Modeling the diffusion of flammable hydrogen cloud under different liquid hydrogen leakage conditions in a hydrogen refueling station. *Int. J. Hydrogen Energy* **2022**, *47*, 25849–25863. [CrossRef]

119. Jeon, J.; Kim, Y.S.; Jung, H.; Kim, S.J. A mechanistic analysis of H_2O and CO_2 diluent effect on hydrogen flammability limit considering flame extinction mechanism. *Nucl. Eng. Technol.* **2021**, *53*, 3286–3297. [CrossRef]

120. Shang, S.; Bi, M.; Zhang, K.; Li, Y.; Gao, Z.; Zhang, Z.; Li, X.; Zhang, C.; Gao, W. Suppression of hydrogen-air explosions by isobutene with special molecular structure. *Int. J. Hydrogen Energy* **2022**, *47*, 25864–25875. [CrossRef]

121. Shang, S.; Bi, M.; Zhang, K.; Li, Y.; Gao, Z.; Zhang, Z.; Li, X.; Zhang, K.; Gao, W. Synergistic effects of isobutene and carbon dioxide on suppressing hydrogen-air explosions. *Int. J. Hydrogen Energy* **2022**, *47*, 25433–25442. [CrossRef]

122. Cao, X.; Zhou, Y.; Wang, Z.; Fan, L.; Wang, Z. Experimental research on hydrogen/air explosion inhibition by the ultrafine water mist. *Int. J. Hydrogen Energy* **2022**, *47*, 23898–23908. [CrossRef]

123. Li, Y.; Bi, M.; Zhou, Y.; Gao, W. Hydrogen cloud explosion suppression by micron-size water mist. *Int. J. Hydrogen Energy* **2022**, *47*, 23462–23470. [CrossRef]

124. Frazier, K. Muskingum River Plant Hydrogen Explosion (PPT). EEI. Retrieved 31 December 2008. Available online: https://www.eei.org/about/meetings/nonav_2007-04-29-cs/Citations_Accident_Review.pdf (accessed on 27 November 2022).

125. *ISO/TS 15869:2009*; Global Technical Regulation (GTR) Nr 13 Global Technical Regulation on Hydrogen and Fuel Cell Vehicles (ECE/TRANS/180/Add.13). ISO: Geneva, Switzerland, 2009. Available online: https://unece.org/transport/standards/transport/vehicle-regulations-wp29/global-technical-regulations-gtrs (accessed on 27 November 2022).

126. *ISO 23273-2: 2006*; Fuel Cell Road Vehicles. Safety Specifications Part 2: Protection against Hydrogen Hazards for Vehicles Fuelled with Compressed Hydrogen. ISO: Geneva, Switzerland, 2006. Available online: https://www.iso.org/standard/41416.html (accessed on 27 November 2022).

127. Directive 2014/94/eu of the European Parliament and of the Council of 22 October 2014 on the Deployment of Alternative Fuels Infrastructure 2014/94/UE (EOG) L 307/1. Available online: https://eur-lex.europa.eu/search.html?qid=1536662083562&text=Directive%202014/94/eu%20of%20the%20European%20Parliament%20and%20of%20the%20Council&scope=EURLEX&type=quick&lang=en (accessed on 27 November 2022).

128. ISO TC 242 Date: 2009/6/17 ISO/CD 50001 ISO PC 242 Secretariat: ANSI Energy Management Systems—Requirements with Guidance for Use SEE International. SAE J2719, Hydrogen Fuel Quality for Fuel Cell Vehicles. Available online: https://www.sae.org/standards/content/j2719_202003/ (accessed on 27 November 2022).

129. *ISO 14687-2.2012*; Hydrogen Fuel, Product Specification, Part 2: Proton Exchange Membrane (PEM) Fuel Cell Applications for Road Vechicles. International Organisation for Standardization: Geneva, Switzerland, 2012. Available online: https://www.sis.se/api/document/preview/915573 (accessed on 27 November 2022).

130. *ISO 22734-1:2008*; Hydrogen Generators Using Water Electrolysis Process—Part 1: Industrial and Commercial Applications. ISO: Geneva, Switzerland, 2008. Available online: https://www.iso.org/standard/41043.html (accessed on 27 November 2022).

131. *ISO 11439-2014*; Gas Cylinders. High Pressure Cylinders for the On-Board Storage of Natural Gas as a Fuel. Specifications. ISO: Geneva, Switzerland, 2014. Available online: https://www.iso.org/standard/44755.html (accessed on 27 November 2022).

132. *ASME STP/PT-0003*; Hydrogen Standardization Interim Report for Tanks, Piping and Pipelines. ASME: New York, NY, USA, 2005. Available online: https://www.techstreet.com/standards/asme-stp-pt-003?product_id=2006093 (accessed on 27 November 2022).

133. *ISO 11114*; 'Transportable Gas Cylinders—Compatibility of Cylinder and Valve Materials with Gas Contents'. International Organization for Standardization: Geneva, Switzerland, 2012. Available online: https://standards.iteh.ai/catalog/standards/cen/b5a48da0-fdcd-45b0-bbac-c92b4728e6bd/en-iso-11114-1-2012 (accessed on 27 November 2022).

134. *ISO Standard 11114–4:2002*; Transportable Gas Cylinders—Compatibility of Cylinders and Valves Materials with Gas Contents—Part 4: Test Methods for Selecting Metallic Materials Resistant to Hydrogen Embrittlement. ISO: Geneva, Switzerland, 2017. Available online: https://standards.iteh.ai/catalog/standards/cen/ee45efeb-9acc-46f4-a588-4e19ff7af441/en-iso-11114-4-2017 (accessed on 27 November 2022).

135. Management System Standards: Comparison Between IAEA GS-R-3 AND ISO 9001:2008 (Safety Reports Series N 69). International Atomic Energy Agency: Vienna, Austria, 2012. Available online: https://www.iaea.org/publications/8706/management-system-standards-comparison-between-iaea-gs-r-3-and-iso-90012008 (accessed on 27 November 2022).

136. Safety Classification of Structures, Systems and Components in Nuclear Power Plants (IAEA Safety Standards Series No. SSG-30). International Atomic Energy Agency: Vienna, Austria, 2014. Available online: https://www-pub.iaea.org/MTCD/publications/PDF/Pub1639_web.pdf (accessed on 27 November 2022).

137. Managing Environmental Impact Assessment for Construction and Operation in New Nuclear Power Programmes (IAEA Nuclear Energy Series No. NG-T-3.11). International Atomic Energy Agency: Vienna, Austria, 2014. Available online: https://www.iaea.org/publications/10391/managing-environmental-impact-assessment-for-construction-and-operation-in-new-nuclear-power-programmes (accessed on 27 November 2022).

138. Blazejewski, W.; Gasior, P.; Kaleta, J. Application of Optical Fibre Sensors to Measuring the Mechanical Properties of Composite Materials and Structures. In *Advances in Composite Materials Ecodesing and Analysis*; Attaf, B.R., Ed.; InTech: London, UK, 2011. [CrossRef]

139. Gasior, P.; Blazejewski, W.; Kaleta, J. Smart fibre optic methods for structural health monitoring of high pressure vessels for hydrogen storage. In Proceedings of the WHEC—World Hydrogen Energy Conference, Essen, Germany, 16–21 May 2010. Available online: https://core.ac.uk/download/pdf/34994657.pdf (accessed on 27 November 2022).

140. Kaleta, J.; Blazejewski, W.; Gasior, P.; Rybaczuk, I. Optimisation of the IV generation tanks for hydrogen storage applied in vehicles. Modelling and experiment. In Proceedings of the WHEC—World Hydrogen Energy Conference, Essen, Germany, 16–21 May 2010. Available online: https://core.ac.uk/download/pdf/34994532.pdf (accessed on 27 November 2022).

141. Balyts'kyi, O.I.; Kawiak, M.; Kawiak, P. Technical diagnostics of the state of the composite evaporators of sulfuric acid. *Mate. Sci.* **2016**, *51*, 727–733. [CrossRef]

142. Balitskii, A.; Semerak, M.; Balitska, V.; Subota, A.; Wus, O. Hydrogen degradation of the pressure gas tanks materials after long-term service. *Solid State Phenomena* **2015**, *225*, 39–44. [CrossRef]

143. Li, H.; Cao, X.; Liu, Y.; Shao, Y.; Nan, Z.; Teng, L.; Peng, W.; Bian, J. Safety of hydrogen storage and transportation: An overview on mechanisms, techniques, and challenges. *Energy Rep.* **2022**, *8*, 6258–6269. [CrossRef]

144. Balyts'kyi, O.I. Two methods of investigation of the influence of hydrogen on the propagation rate of a crack and behavior of fracture of high-strength steels. *Mater. Sci.* **1998**, *34*, 574–583. [CrossRef]

145. Gardiner, M.; Satyapal, S. Energy Requirements for Hydrogen Gas Compression and Liquefaction as Related to Vehicle Storage Needs. DOE Hydrogen and Fuel Cells Program Record. 2009. Available online: https://www.hydrogen.energy.gov/pdfs/9013_energy_requirements_for_hydrogen_gas_compression.pdf (accessed on 27 November 2022).

146. Thomas, C. Fuel cell and battery electric vehicles compared. *Int. J. Hydrogen Energy* **2009**, *34*, 6005–6020. [CrossRef]

147. Mori, D.; Hirose, K. Recent challenges of hydrogen storage technologies for fuel cell vehicles. *Int. J. Hydrogen Energy* **2009**, *34*, 4569–4574. [CrossRef]

148. Gye, H.-R.; Seo, S.-K.; Bach, Q.-V.; Ha, D.; Lee, C.-J. Quantitative risk assessment of an urban hydrogen refueling station. *Int. J. Hydrogen Energy* **2019**, *44*, 1288–1298. [CrossRef]

149. Xu, W.; Li, Q.; Huang, M. Design and analysis of liquid hydrogen storage tank for high-altitude long-endurance remotely-operated aircraft. *Int. J. Hydrogen Energy* **2015**, *40*, 16578–16586. [CrossRef]

150. Babac, G.; Sişman, A.; Çimen, T. Two-dimensional thermal analysis of liquid hydrogen tank insulation. *Int. J. Hydrogen Energy* **2009**, *34*, 6357–6363. [CrossRef]

151. Petitpas, G. Simulation of boilolosses during transfer at a LH2 based hydrogen refueling station. *Int. J. Hydrogen Energy* **2018**, *43*, 21451–21463. [CrossRef]

152. Züttel, A. Materials for hydrogen storage. *Mater. Today* **2003**, *6*, 24–33. [CrossRef]

153. Abdalla, A.M.; Hossain, S.; Nisfindy, O.B.; Azad, A.T.; Dawood, M.; Azad, A.K. Hydrogen production, storage, transportation and key challenges with applications: A review. *Energy Convers. Manag.* **2018**, *165*, 602–627. [CrossRef]

154. Durbin, D.; Malardier-Jugroot, C. Review of hydrogen storage techniques for on board vehicle applications. *Int. J. Hydrogen Energy* **2013**, *38*, 14595–14617. [CrossRef]

155. Muradov, N.; Vezirolu, T. From hydrocarbon to hydrogen-carbon to hydrogen economy. *Int. J. Hydrogen Energy* **2005**, *30*, 225–237. [CrossRef]

156. Barreto, L.; Makihira, A.; Riahi, K. The hydrogen economy in the 21st century: A sustainable development scenario. *Int. J. Hydrogen Energy* **2003**, *28*, 267–284. Available online: https://pure.iiasa.ac.at/id/eprint/7086/1/RR-03-001.pdf (accessed on 27 November 2022). [CrossRef]

157. Penner, S.S. Steps toward the hydrogen economy. *Energy* **2006**, *31*, 33–43. [CrossRef]

158. Bossel, U. Does a hydrogen economy make sense? *Proc. IEEE* **2006**, *94*, 1826–1837. [CrossRef]

159. ITM Power. Hydrogen Refuelling Infrastructure. 2017. Available online: http://www.level-network.com/wpcontent/uploads/2017/02/ITM-Power.pdf (accessed on 27 November 2022).

160. Lin, H.; Yang, M.; Shu, B. Fretting wear behaviour of high-nitrogen stainless bearing steel under lubrication condition. *J. Iron Steel Res. Int.* **2020**, *27*, 849–866. [CrossRef]

161. Hutsaylyuk, V.; Student, M.; Dovhunyk, V.; Posuvailo, V.; Student, O.; Maruschak, P.; Koval'chuck, I. Effect of hydrogen on the wear resistance of steels upon contact with plasma electrolytic oxidation layers synthesized on aluminum alloys. *Metals* **2019**, *9*, 280. [CrossRef]

162. Osenin, Y.I.; Sosnov, I.I.; Chesnokov, A.V.; Antoshkina, L.I.; Osenin, Y.Y. Friction unit of a disc brake based on a combination of friction materials. *J. Frict. Wear* **2019**, *40*, 193–196. [CrossRef]

163. Pokhmurs'Kyi, V.I.; Vasyliv, K.B. Influence of hydrogen on the friction and wear of metals (a survey). *Mater. Sci.* **2012**, *48*, 125–130. [CrossRef]

164. Banks, D.; Clayton, P. Comparison of the wear process for eutectoid rail steels: Field and. laboratory tests. *Wear* **1987**, *120*, 233–250. [CrossRef]

165. Clayton, P. Predicting the wear of rails on curves from laboratory data. *Wear* **1995**, *181–183*, 11–19. [CrossRef]

166. Tkachov, V.I.; Levina, I.M.; Ivas'kevych, L.M. Distinctive features of hydrogen degradation of heat-resistance alloys based on nickel. *Mater. Sci.* **1997**, *33*, 524–531. [CrossRef]

167. Fragin, M.; Leyzerovich, A.; Shapiro, M. Fire-resistant fluids seek to expand application into turbine lubrication systems. *Power Eng.* **2001**, *105*, 106–115. Available online: https://go.gale.com/ps/i.do?id=GALE%7CA80864944&sid=googleScholar&v=2.1&it=r&linkaccess=abs&issn=00325961&p=AONE&sw=w&userGroupName=anon%7Efa0b0f82 (accessed on 27 November 2022).

168. Pan Guo Wei, P.G.; Xu, H.Z. A mini NMR sensor for monitoring the degradation of fire-resistant turbine oils in thermal power plant in vivo. *Prog. Electromagn. Res. C* **2014**, *55*, 1–7. [CrossRef]

169. Vilyanskaya, G.D.; Lysko, V.V.; Fragin, M.S. Improving fire prevention in turbine plants by using fire-resistant oils. *Therm. Eng.* **1988**, *35*, 193–195.

170. Vilyanskaya, G.D.; Lysko, V.V.; Phillips, W.D. Recent operating experience in Europe and the Soviet Union with fire-resistant turbine lubricants. *Proc. Am. Power Conf.* **1990**, *52*, 704–708.

171. Vilyanskaya, G.D.; Lysko, V.V.; Fragin, M.S.; Vainstein, A.G. VTI Fire-resistant turbine oils and the part played by them in increasing fire protection at thermal and nuclear power stations. *Therm. Eng.* **1991**, *38*, 38–41.

172. Gunther, R. Operating experience with synthetic fluids in the control and governing systems of steam turbines. *VGB PowerTech* **1997**, *77*, 30–934.

173. Schenk, K.; Hunxtermann, E.; Hartwig, J. Operation of turbines with fire-resistant fluids, including the lubrication system. *Int. Joint Power Gener. Conf. ASME* **1998**, *2*, 799–806.

174. Phillips, W.D. The use of a fire-resistant turbine lubricant: Europe looks to the future. In Proceedings of the ASTM Conference Turbine Lubrication in the 21st Century, West Conshohocken, PA, USA, 10–14 January 2001.

175. Electric Generating Plants and High Voltage Direct Current Converter Stations. NFPA Standard 850-24, 1996, Section 6-5.3.3. Recommended Practice for Fire Protection for Electric Generating Plants and High Voltage Direct Current Converter Stations. Available online: https://www.nfpa.org/codes-and-standards/all-codes-and-standards/list-of-codes-and-standards/detail?code=850 (accessed on 27 November 2022).

176. Strušnik, D. Integration of machine learning to increase steam turbine condenser vacuum and efficiency through gasket resealing and higher heat extraction into the atmosphere. *Int. J. Energy Res.* **2022**, *46*, 3189–3212. [CrossRef]